JOURNAL OF GEOPHYSICAL RESEARCH, VOL. 97, NO. C1, PAGES 769–788, JANUARY 15, 1992

Separation of Tidal and Subtidal Currents in Ship-Mounted Acoustic Doppler Current Profiler Observations

JULIO CANDELA,[1] ROBERT C. BEARDSLEY, AND RICHARD LIMEBURNER

Department of Physical Oceanography, Woods Hole Oceanographic Institution, Woods Hole, Massachusetts

A simple method is developed to analyze current measurements obtained from a moving platform. The need for this is motivated by the now common use of the ship-mounted acoustic Doppler current profiler (ADCP) to acquire absolute velocity data during an oceanographic survey of a given region. The full potential of this new measurement technique is severely hindered when the presence of high-frequency phenomena (e.g., tidal or inertial motions) prevents a clear visualization of the lower-frequency current structure of interest. Our analysis method is based on a spatial interpolation scheme, using arbitrary functions, that allows for the tidal current time variability, which then permits the tide-induced motions to be subtracted from the ADCP data to yield the subtidal current field. The method also allows nearby moored and drifter current measurements (if available) to be combined with the shipboard ADCP observations in a single analysis to obtain the best description of the tidal and subtidal currents. To illustrate this method, we present results from the analysis of ADCP data taken during oceanographic surveys in two different continental shelf regions, the East China Sea and the Amazon shelf. A 5-day conductivity-temperature-depth (CTD) and ADCP survey was made in the East China Sea near the mouth of the Yellow Sea during January 1986. There the currents were essentially barotropic and dominated by the semidiurnal tide. The ADCP-derived cotidal chart for the M_2 (12.42 hours) component agrees well with existing charts derived empirically from sea level observations or from regional numerical models. The ADCP-derived steady flow is also consistent with the observed density field and indicates little flow in or out of the Yellow Sea and a transport of about 1 Sv toward the Tsushima Strait. Two CTD–ADCP surveys lasting 21 and 23 days were conducted over the Amazon shelf during March and May, 1990. Simultaneously moored current observations were also obtained at three locations along a cross-shelf array 200 km north of the Amazon River mouth, for a common period of at least 2 months (February 12 to April 13). Over the shelf, tidal and subtidal currents were comparable in magnitude. Our analysis indicates that the tidal currents were essentially barotropic, semidiurnal, and polarized in the cross-shelf direction, increasing in magnitude toward the inner shelf where current values of more than 2 m/s are common. The ADCP-derived steady currents were aligned in the along-shelf direction and strongly influenced by the North Brazil Current (NBC). During both ADCP surveys, the northwestward flowing NBC was transporting more than 2 Sv over the shelf at depths shallower than 100 m.

1. INTRODUCTION

The acoustic Doppler current profiler (ADCP) combined with accurate navigation has revolutionized the way ocean currents are measured. Mounted on a ship, this instrument provides a quasi-continuous vertical profile of horizontal current along the ship's track. Ideally, this should allow one to determine the tidal and subtidal patterns of circulation from a regional survey spanning a few days. However, even if one is not interested in the tidal dynamics of the region but is interested only in the subtidal circulation, the presence of tidal variability in the ADCP data is unavoidable, especially in coastal regions where the tide can be the dominant current signal present. Thus the intrinsic contamination of the ADCP data by tidal components is a serious problem that can render the data useless unless an analysis method is devised to filter out the tidal variability. The source of this problem is due to the spatial variation of the tidal wave, which does not permit a simple harmonic analysis procedure as when dealing with time series measurements taken at a fixed point in space.

To date, two basic ways to deal with this problem have been proposed. The first approach relies on designing the sampling survey in a way that permits measuring at the same location several times in order (1) to have enough samples to safely average out the tide [*Kosro*, 1985], or (2) to have enough samples over a single tidal period to construct time series of the currents at each chosen location, so that a harmonic analysis may be performed on the data [*Geyer and Signell*, 1990; *Lwiza and Bowers*, 1990; *Simpson et al.*, 1990]. Unless there are more specific reasons to follow an intensively repetitive survey track other than to account for the tides, this procedure represents a very inefficient use of ship time. The second approach is to make use of tidal current predictions from either (1) a numerical model of the region under study [*Foreman and Freeland*, 1991] or (2) previous knowledge of the region, where enough moored observations are available, to permit a reasonable interpolation of the tidal currents at the ADCP observation locations along the ship's track [*Münchow et al.*, 1991]. Procedure 1 has had limited application so far, since its use is restricted to regions where the observed tidal currents are well simulated by an existing numerical model. Procedure 2 seems to work well, although it is restricted to areas where enough current data is available from previous work to reasonably map the tidal current structure in the region surveyed with the ADCP. Even in these latter cases, we will argue in section 4 that combining existing data with those available from the ADCP survey should provide a better interpolation for the tidal currents than analyzing each data source separately.

[1]Also at Dirección General de Oceanografía Naval, Secretaría de Marina, México.

Paper number 91JC02569.
0148-0227/92/91JC-02569$05.00

We have investigated an alternative approach to the problem extending previous work by *Candela et al.* [1990]. Our primary interest is in developing a method that treats a one-realization survey of an area in order to remove the principal tidal variance present in the ADCP data and properly reveal the subtidal circulation pattern. Rather than just a filtering technique, our method also gives estimates of the spatial structure of the principal tidal constituents for the region under study. We believe that an analysis approach like that described in section 2 is not restricted to cases where the tidal variability dominates, but could be also used in deep ocean surveys where the source of the high-frequency variability might be principally inertial. The application of the method is possible as long as frequency spectra of segments of the survey reveal a well defined spectral gap between the high-frequency noise and the lower frequency signal, and as long as the spatial scale of the noise is not too small. Under such conditions, the analysis method should also provide some information about the spatial scales of the inertial oscillations within the region surveyed.

This paper is organized as follows. The basic analysis method will be described next in section 2. Section 3 describes the application of this method to ADCP data sets from the East China Sea and the Amazon shelf. Current measurements were also made at anchor stations and with moorings over the Amazon shelf, and the effect of combining these data with the ADCP data will be discussed also in section 3. The conclusions from this work are summarized in section 4.

2. THE METHOD

When observations of currents over a few days are available at a given location, it is always possible to represent them by a function of the form

$$\begin{aligned} u(t) &= u_0 + \sum_{i=1}^{N} a_i \cos(\omega_i t - \theta_i) \ , \\ &= u_0 + \sum_{i=1}^{N} [b_i \cos(\omega_i t) + c_i \sin(\omega_i t)] \ , \end{aligned} \qquad (1)$$

where

$$\begin{aligned} a_i &= ({b_i}^2 + {c_i}^2)^{1/2} \ , \\ \theta_i &= \arctan\left(\frac{c_i}{b_i}\right) \ , \end{aligned}$$

$u(t)$ is the time series of observed eastward current component at a given location and depth, u_0 is its mean over the observation interval, and ω_i, a_i, and θ_i are the frequency, amplitude, and phase of the ith tidal constituent, of which there are N included in the representation. N depends in part on the length of the observations, which determines the resolution among possible constituents in accordance with a previous knowledge of the hierarchy of constituents to use in the region under study. A similar representation is possible for the north component $v(t)$.

This representation allows us to remove the tidal variability from the current records by projecting the observations onto (1), using a least squares requirement on the residuals. This procedure is not directly applicable in the case where the data is also a function of the horizontal coordinates (x, y), as is the case with ship-mounted ADCP data. The spatial scales of this variation depend on the spatial structure of the tidal and subtidal flow in the particular area being surveyed. While perhaps larger in the deep ocean, these scales can be quite short, even less than a few kilometers, in some coastal regions.

One simple solution to this problem is to allow for the tidal spatial variability in a representation similar to (1), i.e., allow a and θ or similarly b and c in (1) to be functions of x and y. Although there are particular functions (the normal modes) preferred by the tidal wave in a given bathymetric configuration, we will attempt to approximate the tidal spatial structure using arbitrary interpolating functions. In general, u_0 and v_0 might also vary spatially over the surveyed region; therefore they too should be considered functions of x and y. In this paper we will refer to the steady field as that part of the measurements which we considered time invariant over the length of the observations, but possessing a spatial variability which we will also try to resolve with the aid of arbitrary spatial interpolating functions. Thus if our removal of the tidal variability from the subtidal component is perfect, the subtidal current field will consist of the mean steady field (u_0 and v_0) and a residual field caused by the unresolved subtidal temporal and spatial variability. The representativeness of the steady current component and its interpretation are of course critical scientific questions which must be addressed with all available knowledge and physical intuition about the regional general circulation.

Perhaps the simplest interpolating functions are polynomials in powers of x and y. These have been used extensively in geology for approximating spatial structures of geologic formations, and the procedure is commonly referred to as trend surface analysis [*Davis*, 1986]. Specifically, in our application we expand b_i (and u_0 and c_i) in (1) as

$$b_i(x, y) = \sum_{j=0}^{DP} \sum_{k=0}^{j} \alpha_\ell x^{j-k} y^k \ , \qquad (2)$$

where the values of α are constants to be fit to the observations, DP the degree of the polynomial, and j and k are integers with $\ell = (j-k, k)$. This type of polynomial is simple and flexible to use, but for $DP > 1$, it tends to be badly behaved at the edges of the interpolating region and beyond, therefore preventing its use as an extrapolating function.

A second set of commonly used interpolating functions are the Green function solutions of the biharmonic equation whose general solution can be expressed as the linear combination [*Sandwell*, 1987]

$$b_i = \sum_{j=1}^{K} \beta_j \phi(\mathbf{x}_i - \mathbf{x}_j) \ , \qquad (3)$$

where $\mathbf{x}_i \neq \mathbf{x}_j$ and

$$\phi(\mathbf{x}) = |\mathbf{x}|^2 (\ln|\mathbf{x}| - 1) \qquad (4)$$

is the biharmonic Green function in two dimensions. If we consider all the data points m in solving for the values of β in (3), i.e., $K = m$, we obtain an interpolation practically indistinguishable from the common spline interpolation. In our case, the aim is not to fit the data exactly at every measurement point, but rather to minimize some measure of the deviations of the approximating functions to the actual data values. This can be simply done by altering the

summation in (3) to reduce the number of model parameters used, or by arbitrarily specifying K locations ($\mathbf{x}_j$ called knots) in and/or near the surveyed area, with K less than the total number of observations. By doing this, we end up with an overdetermined system of equations that can be solved by imposing a least squares requirement. The interpolating function so obtained is a smoothed version of the common spline fit. Contrary to the polynomial interpolation, the biharmonic interpolation is very flexible over the region where data is available, but behaves smoothly everywhere else. Some caution should be exercised when using biharmonic functions as basis because the resulting interpolation is dependent not only on the number (K) but also on the actual locations of the knots. This is more evident when calculating the elevation cotidal charts from the fitted tidal transports. Although we tried several numerical schemes to automatically pick the knot locations on the basis of the initial data distribution, none were completely satisfactory, and eventually a good degree of experimentation was required to select the best knot locations to get appealing results.

Irrespective of the basis function chosen, the system of equations to be solved is of the form

$$\mathbf{A}\mathbf{c} = \mathbf{d} \quad , \tag{5}$$

where $\mathbf{A}$ is a $(m \times n)$ model matrix which depends on the basis functions chosen, with m being the number of observation points and n the model order, $\mathbf{c}$ is an n column vector of unknown coefficients, and $\mathbf{d}$ is an m column vector containing the measurements. (We have chosen to pose this least squares problem in matrix notation so that it can be readily coded and solved using the matrix language MATLAB.) In practice there will be separate systems of equations for the u (east) and v (north) components, both with identical $\mathbf{A}$ matrices but different $\mathbf{c}$ and $\mathbf{d}$ vectors. Formally, the solution to (7) is given by $\mathbf{c} = (\mathbf{A}^T\mathbf{A})^{-1}\mathbf{A}^T\mathbf{d}$; however, the explicit calculation of $\mathbf{A}^T\mathbf{A}$ and its inverse might lead to large inaccuracies due to rounding errors.

A numerically more stable procedure to solve (7) is by first calculating the singular value decomposition (SVD) factorization of the matrix $\mathbf{A}$ [*Forsythe et al.*, 1977], i.e.,

$$\mathbf{A} = \mathbf{U}\mathbf{\Sigma}\mathbf{V}^T \quad , \tag{6}$$

where $\mathbf{U}$ and $\mathbf{V}$ are $(m \times m)$ and $(n \times n)$ orthogonal matrices respectively and $\mathbf{\Sigma}$ is a $(m \times n)$ diagonal matrix containing the singular values, i.e., the positive square roots of the eigenvalues of the product $\mathbf{A}^T\mathbf{A}$.

This method has the additional advantage of permitting the elimination of near singularities in $\mathbf{A}$. These might appear if the basis functions used are linearly dependent at the data points, resulting in linear dependent columns in $\mathbf{A}$. It turns out that the singular values (σ) are nonzero if and only if the basis functions are linearly independent at the data points, therefore an appropriate condition number for $\mathbf{A}$ is given by $(\sigma_{\max}/\sigma_{\min})$, i.e., the ratio of the largest to the smallest singular values. Since the condition number is an error magnification factor, in ill-conditioned cases, the elimination of all $\sigma_i \leq \kappa$, where κ is an error tolerance value, gives a more reliable determination of $\mathbf{c}$ although with a possible increase in the size of the residuals. Usually, the error tolerance κ is chosen to reflect the rounding error expected in the computations and is given by $\kappa = m\epsilon\sigma_{\max}$, where ϵ is the machine epsilon (2^{-52} in our case). This value of κ is strictly valid for exact data, which in oceanography is never the case. It could be argued that in practical situations a larger value for κ, somewhat related to the actual data accuracy, would be more appropriate. However, our practical recommendation is that irrespective of the value of κ, the condition number for $\mathbf{A}$ should always be kept reasonably small, say less than 10^4, by either rescaling the independent variables, reducing the model order, or choosing a completely different set of basis functions. For all the examples treated in this paper, the highest matrix condition encounter was 2×10^3 and singular value editing was never used. Thus from a statistical point of view, all the results shown here are the natural solution of the system of equations posed.

Specifically the solution procedure is straightforward, with the least squares approximation of $\mathbf{c}$ given by

$$\hat{\mathbf{c}} = \mathbf{V}\mathbf{\Sigma}^{-1}\mathbf{U}^T\mathbf{d} \quad , \tag{7}$$

where $\mathbf{\Sigma}^{-1}$ is the pseudo-inverse of the matrix $\mathbf{\Sigma}$, i.e., a $(m \times n)$ diagonal matrix whose elements are those of $\mathbf{\Sigma}$ to the -1 power (for details see *Lawson and Hanson* [1974, chap. 7]). For the determination of error estimates in the model, it is important to calculate the covariance matrix of the coefficients $\hat{\mathbf{c}}$, in the formal solution expressed by $(\mathbf{A}^T\mathbf{A})^{-1}$, but in our case given by

$$\mathbf{C} = \mathbf{V}\mathbf{\Sigma}^{-2}\mathbf{V}^T \quad , \tag{8}$$

where $\mathbf{\Sigma}^{-2} = (\mathbf{\Sigma}^T\mathbf{\Sigma})^{-1}$. Once $\hat{\mathbf{c}}$ is determined, the product $\mathbf{A}\hat{\mathbf{c}} = \hat{\mathbf{d}}$ gives the model estimate $\hat{\mathbf{d}}$ which represents the projection of the data onto the space expanded by the columns of $\mathbf{A}$. The corresponding misfit or residual is then $\epsilon = \mathbf{d} - \hat{\mathbf{d}}$, with variance $\vartheta = \epsilon^T\epsilon/(m-n)$. To obtain an unbiased variance estimate, it is necessary to calculate the true degrees of freedom (ν) of the measurements. This brings up the need to know the spatial and temporal decorrelation scales in the measurements, which, with just one realization survey of an area, are not resolved. The best we can do is to integrate the autocorrelation function of the observations $\mathbf{d}$, taking them as if only time dependent, to obtain the degree of independence among points in the data set at hand. Even so, these decorrelation scales only make sense for the subtidal variability, since for a narrow-band process such as the tides, the autocorrelation function is periodic. Supposing that this measure of the degree of statistical independence in the ADCP data is reasonable, the true number of degrees of freedom is given by $\nu = (m\Delta t/\tau) - n$, where τ is the integral of the autocorrelation function of the detided observations and Δt the time averaging interval chosen. This leads to an unbiased variance estimate for the model given by $\hat{\vartheta} = \epsilon^T\epsilon/\nu$.

If $\mathbf{d}$ is assumed a random variable normally distributed about a true value $\mathbf{d}_t$ with variance $\hat{\vartheta}$, the coefficients in $\hat{\mathbf{c}}$ will also be normal random variables with variance $\hat{\vartheta}_{\mathbf{c}} = \hat{\vartheta}\,\mathrm{diag}(\mathbf{C})$, where $\mathrm{diag}(\mathbf{C})$ is a vector containing the diagonal elements in $\mathbf{C}$, *i.e.*, the autocovariances of the coefficients. Accordingly, estimates in $\hat{\mathbf{d}}$ are also normally distributed about a true value with a variance

$$\hat{\vartheta}_{\hat{\mathbf{d}}} = \hat{\vartheta}\,\mathrm{diag}(\mathbf{A}\mathbf{C}\mathbf{A}^T) \quad . \tag{9}$$

We can use this latter expression to compute standard deviation estimates for $\hat{\mathbf{d}}$; however, extending our statistical analysis a bit further, we notice that for a normally distributed $\hat{\mathbf{d}}$, the ratio $\hat{\mathbf{d}}/\sqrt{\hat{\vartheta}_{\hat{\mathbf{d}}}}$ has a "Student's t" distribu-

tion with ν degrees of freedom. This permits us to supply the estimate $\hat{\mathbf{d}}$ with appropriate confidence limits to the desired percentage.

Before the applications are shown, some thought has to be given to the actual construction of the model matrix **A**. Although there is a finite number of tidal constituents that can potentially be resolved from a data set spanning a specific length of time [*Godin*, 1972], the degree of the polynomials (DP) in (2) or the number of chosen knots (K) in (3) is arbitrary for each of the resolvable tidal constituents as well as for the steady part of the representation. Thus the number of possible combinations of components and term orders entering the construction of **A** is quite large. It is therefore helpful to use any prior knowledge of the region under study and also to conduct some experimental trials. Once the number of components appropriate to the given data set has been agreed upon, the search for the optimal order, i.e., DP in (2) and K in (3), for each of the terms can be guided by a statistical F test. The F test, which is robust even for data not perfectly normally distributed, is based on the variance ratio $[(SSM_{p+1} - SSM_p)/(dn_{p+1} - dn_p)]/[SSR_{p+1}/dm_{p+1}]$, where SSM is the sum of squares of the model estimate ($\hat{\mathbf{d}}$), SSR is the sum of squares of the residual (ε), dn is the number of columns in **A** (n) for orders $p+1$ or p, and $dm_{p+1} = m - n_{p+1} - 1$. This ratio simply indicates that if the model variance does not increase more rapidly than the residual variance as the order p is increased, then the new features explained by the model are as apt to be noise or signal and the analysis is not improved. Unfortunately, if the model consists of more than one component, the outcome of the F test, when searching for the significance of increasing the order, depends on the search path followed. Therefore the optimal model order can not be found by an automatic procedure, and the search path has to be prespecified according to prior knowledge of the relative importance of the components constituting the model matrix in relation to the data. In our application we found the F test useful for setting objective upper limits for the model order; however, its results tended to be overoptimistic at times, pushing the order to the limit where the model started to misbehave. Therefore the F test is a useful guide for setting the model order, but its results should be critically examined.

3. Application to East China Sea and Amazon Shelf Data Sets

3.1. *The East China Sea*

First we will analyze data from an ADCP and conductivity-temperature-depth (CTD) survey conducted in the East China Sea near the mouth of the Yellow Sea in January 1986 (Figure 1). The Yellow Sea is broad (~ 500 km) and shallow (~ 50 m average depth), and is well known for its strong semidiurnal tidal currents and surface tides [*Choi*, 1980]. The regional subtidal circulation is thought to

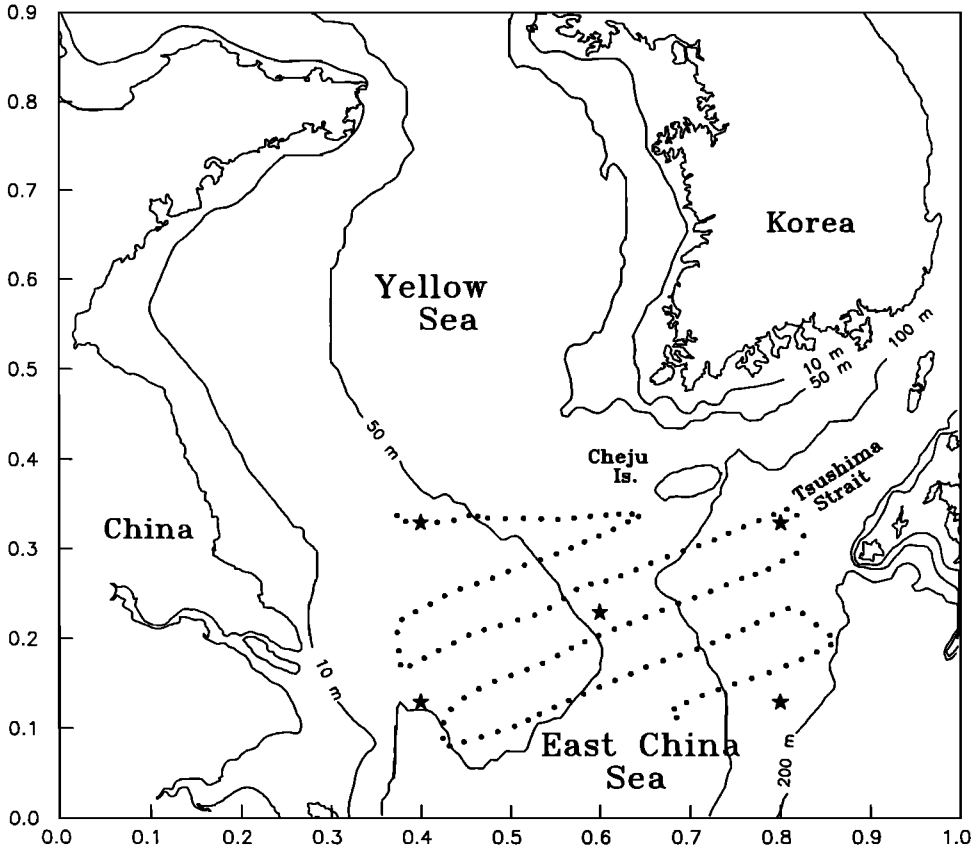

Fig. 1. Map of the East China and Yellow seas. The coordinate axes are in thousands of kilometers, i.e., 100 km per tick mark, with the origin (0,0) at 119°E, 30°N. Shown by dots are the main ADCP stations used in the analyses presented. The 129 stations are roughly 1 hour apart in time along the ship's track which started at the northwesternmost station. The data shown were collected during January 24–29, 1986. The 10-, 50-, 100-, and 200-m isobaths are shown. The five stars indicate the locations of the knots used in the biharmonic basis functions representation.

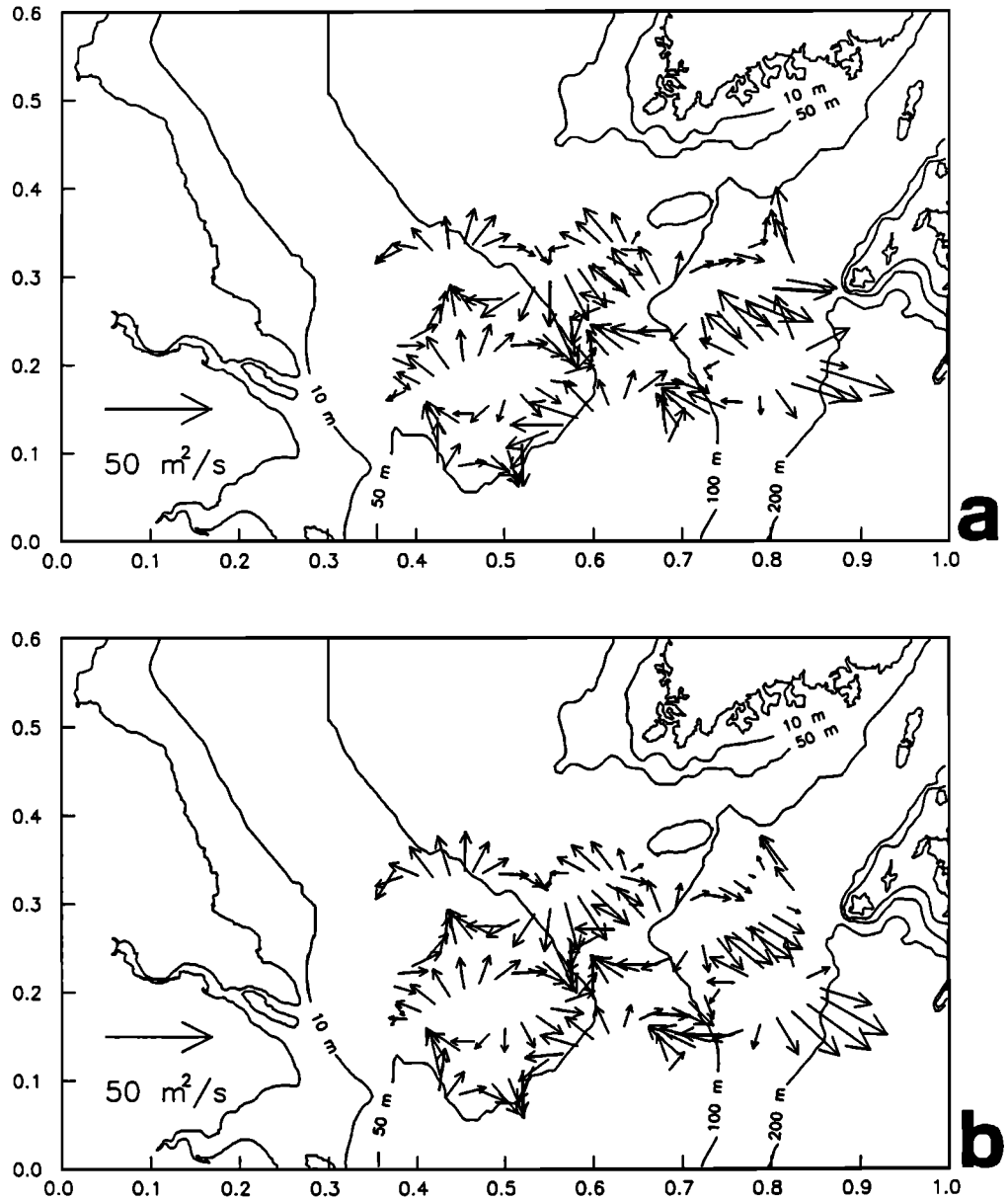

Fig. 2. Subsection of the map in Figure 1 containing the mouth of the Yellow Sea region. The axis scaling is as in Figure 1, i.e., 100 km per tick mark with the origin at 119°E, 30°N. (*a*) Total vertically integrated ADCP data or total transport at the stations indicated in Figure 1. The units are square meters per second, with the scale given in the lower left-hand corner. (*b*) Fitted tidal transport to the observations in Figure 2*a*. The approximation is made by expanding the spatial variability of the semidiurnal component with a second-degree polynomial and a first degree for the diurnal tide.

be much weaker than the tidal currents, which makes this a good region to test the performance of the method proposed above. The ADCP data were obtained with a 150-kHz RDI ADCP mounted on the R/V *Thompson* set up with a 4-m vertical bin resolution and a 3-min sampling interval. The ship's absolute motion was determined from bottom tracking which was continuous over the part of the survey analyzed here. The accuracy of the bottom-tracking velocity was examined by comparison with occasional position data obtained with the Global Positioning System (GPS), yielding an estimated uncertainty in hourly averaged ADCP data of about ±1.2% of the true velocity or ±0.5 cm/s, whichever is larger (see appendix).

To obtain smoother samples of the tidal and subtidal processes we are interested in measuring, we chose to define main data stations every hour or every 20 km, whichever came first along the ship's track. The 1-hour time resolution is the common practice in harmonic analysis of tidal time series. The 20-km spatial resolution was chosen after studying the cotidal charts for the region [*Choi*, 1980]. After these time and spatial resolutions were set, all of the 3-min ADCP profiles that fell within the domain of a given main data station were averaged together after elimination of those depth bins, in each profile, with less than 90% of the optimal acoustic power return. To further simplify the analysis, the profile data were averaged in the vertical and multiplied by the lo-

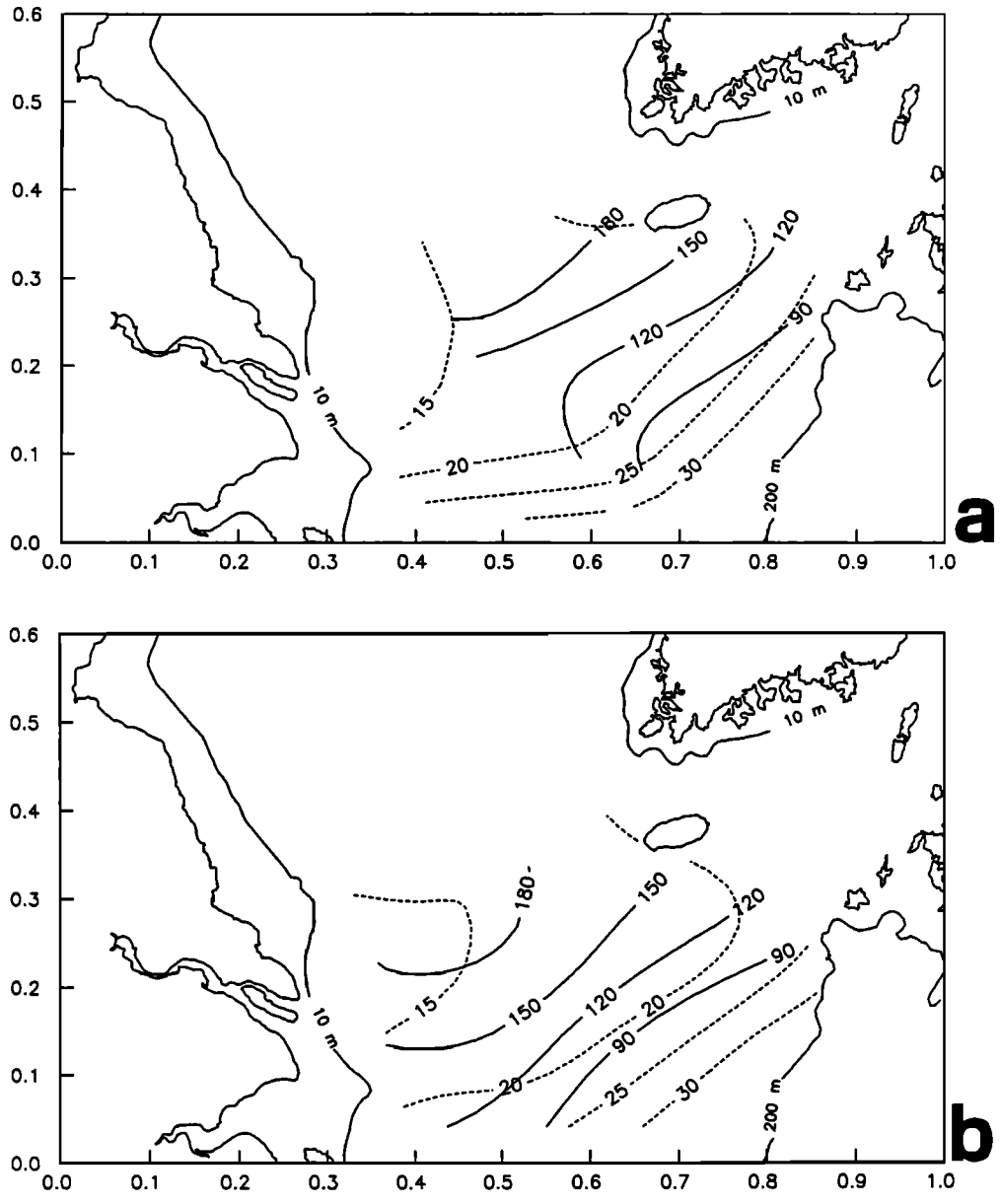

Fig. 3. Contours of semimajor axis (dashed lines, in square meters per second) and phase (solid lines, in degrees with respect to UT) of the semidiurnal M_2 transport ellipse. The analysis is based on (*a*) second-degree polynomial approximation in the spatial coordinates and (*b*) biharmonic basis functions using the five knots shown in Figure 1 by stars.

cal depth to obtain estimates of transport. This procedure is justified because during the winter months the water column is locally homogeneous in the region (C. Chen et al., Comparison of winter and summer hydrographic observations in the Kuroshio and adjacent East China Sea during 1986, submitted to Continental Shelf Research, 1991), and the individual ADCP current profiles showed little vertical shear. The result of this spatial and temporal averaging of ADCP data collected during January 24–29, 1986, defined the 129 stations shown in Figure 1. This survey covered an area roughly 300 by 500 km at the entrance to the Yellow Sea and varied in depth from 30 m (at the westernmost stations) to 200 m (at the easternmost stations).

For a first application of the method, we modeled the vertically integrated transports at the defined stations (see Figure 2*a*) by expanding the horizontal spatial structure of the semidiurnal tide with second-degree polynomials and that of the diurnal tide and the steady transports with first-degree ones. The degrees of the polynomials chosen are guided by the F test described in section 2. For the tidal components we chose the M_2 (28.98°/h) and the K_1 (15.04°/h) frequencies as representative for the semidiurnal and diurnal terms respectively. With only 5 days of data, it is not possible to resolve a pure M_2 or K_1 constituent; instead the fit tends to lump together all the available semidiurnal variability into the M_2 term and all the diurnal variability into the K_1 term. While using average frequencies within each band may be more appropriate than using the M_2 and K_1 frequencies, for the data at hand, small variations in the frequencies used do not make any appreciable difference in the results. Although

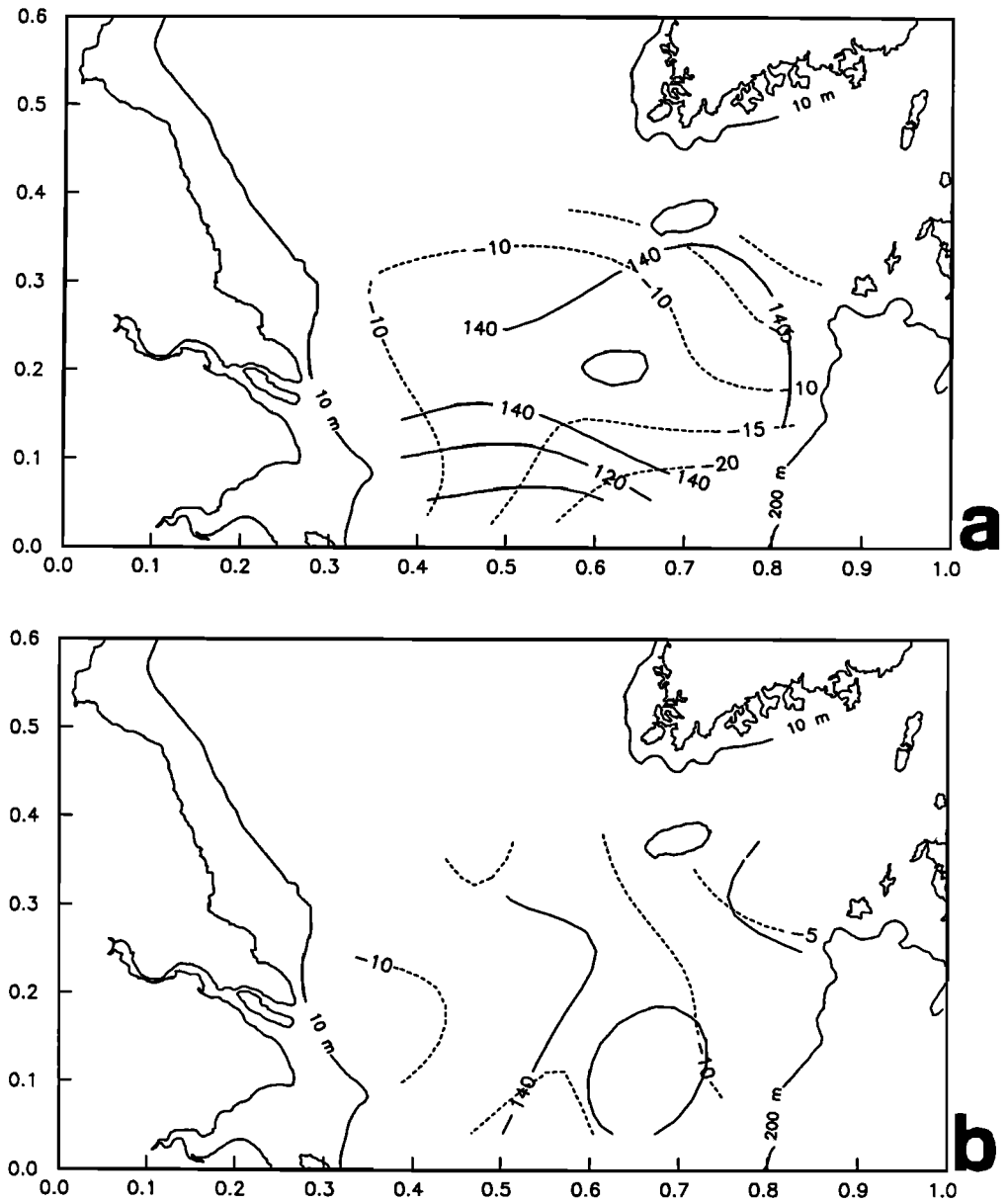

Fig. 4. Contours of semiminor axis (dashed lines, in square meters per second) and orientation (solid lines, in trigonometric degrees with respect to east) of the semidiurnal M_2 transport ellipse. The analysis is based on (*a*) second-degree polynomial approximation in the spatial coordinates and (*b*) biharmonic basis functions using the five knots shown in Figure 1 by stars.

the tide in the East China Sea is principally semidiurnal, the diurnal tide is not negligible ($K_1/M_2 \sim 0.25$ over the survey region), requiring us to include a diurnal term in the fit. Without a diurnal term included, the residual is still contaminated with tidal variability. Figure 2*b* shows the modeled tidal transports obtained with the polynomial expansions of the semidiurnal and diurnal tides. The resemblance to the actual observations is impressive, confirming the dominance of the current field by tidal components. Similar tidal patterns are obtained if biharmonic functions or Kelvin and Poincaré modes are used as basis functions. The subtle differences resulting from using differing basis functions are more evident in computing cotidal charts from the fitted current fields, as will be discussed below.

To synthesize the tidal transport information, we show tidal transport ellipse parameters in Figures 3 and 4. Figure 3 shows contours of the semimajor axis and phase of the transport ellipse for the semidiurnal tidal component. The phase indicates the time of occurrence of the maximum transport value, which refers here to the flooding tide according to the ellipse orientations given in Figure 4. Figure 3*a* is the approximation using a second-degree polynomial; i.e., the semidiurnal part of the tidal transport vectors of Figures 2*b* and 3*b* is that obtained with biharmonic basis functions using five arbitrarily placed knots whose locations are indicated by the stars in Figure 1. The two approximations are very similar, indicating a decrease in transport from the deeper southeastern region towards the shallower northwestern interior. Dividing these transport values by the local depth indicates an increase in the vertically averaged semidiurnal tidal currents from about 0.15 to 0.5 m/s as one moves from the southeast to the northwest through

the survey region. The phase lines show the semidiurnal tidal signal progressing toward the northwest, taking about 5 hours to traverse the survey region. Figure 4 completes the semidiurnal tidal transport ellipse description by showing contours of its semiminor axis and the ellipse orientation or inclination of the semimajor axis with respect to east. Again, Figure 4*a* corresponds to the approximation obtained by polynomials, while Figure 4*b* is that obtained with the biharmonic basis functions. Figure 4 indicates a slight increase in the semiminor axis towards the west and south, the negative sign being indicative of a clockwise rotation of the semidiurnal tidal currents over the survey region. The ellipse orientation, which is measured counterclockwise from the east, indicates that the major axis is principally oriented along the main channel entering the Yellow Sea at about 140°.

A check on how well the tides are being fitted can be provided by constructing cotidal charts for elevation based on the fitted transports. These can be compared with either empirically drawn charts based on coastal and island sea level observations from the surrounding region or with charts obtained with a numerical tidal model of the area. *Choi* [1980] has used the standard Heaps barotropic numerical tidal model to predict semidiurnal and diurnal tides in the East China and Yellow seas. Part of Choi's elevation cotidal chart for M_2 is shown in Figure 5: in the survey region the M_2 surface tide propagates toward the northwest, with amplitude increasing toward the mouth of the Changjiang (Yangtze River). From our fits to the transports, we can compute an elevation cotidal chart for M_2 using the continuity equation

$$-\frac{\partial \eta}{\partial t} = \frac{\partial uh}{\partial x} + \frac{\partial vh}{\partial y} \quad , \tag{10}$$

where η is the sea surface elevation, h is water depth, and t is time. For a tidal constituent, the time derivative in elevation is $i\omega\eta$. Calculation of the divergence terms in (12) from the polynomial or biharmonic fits is straightforward. A derivative intrinsically acts as a high-pass filter, so even if the current cotidal charts compare well irrespective of the basis functions chosen, the elevation cotidal charts obtained through the application of (12) will enhance their dissimilarities.

The M_2 elevation cotidal charts obtained are shown in Figure 6 for both polynomial and biharmonic fits. Contours of elevation amplitude show a tendency to increase in the southwest or south, and lines of equal phase show a clear propagation of the M_2 surface tide towards the northwest. Both charts in Figure 6 are qualitatively similar and also compare well with Choi's results shown in Figure 5. When doing this comparison, one must remember that the charts shown are obtained from only 5 days of data and do not represent a pure M_2 tide but are merely an approximation to the semidiurnal tide present during the survey. Since the ratio of S_2/M_2 amplitude over the survey area is about 0.4, our inability to separate S_2 from M_2 with the data at hand should account for a large part of the discrepancies between Figures 5 and 6. The cotidal chart deduced from polynomials (Figure 6*a*) appears a bit more artificial than that deduced by using the biharmonics (Figure 6*b*); however, from either chart we are able to infer the main tendencies in amplitude and phase displayed by the semidiurnal tide in the region. Comparing Figures 3 and 6, i.e., the amplitude and phase of the semidiurnal tidal transports and elevation over the survey area, the near-zero phase difference between transport and elevation is indicative of the progressive character of the semidiurnal tidal wave as it sweeps northwestward across the continental shelf into the Yellow Sea.

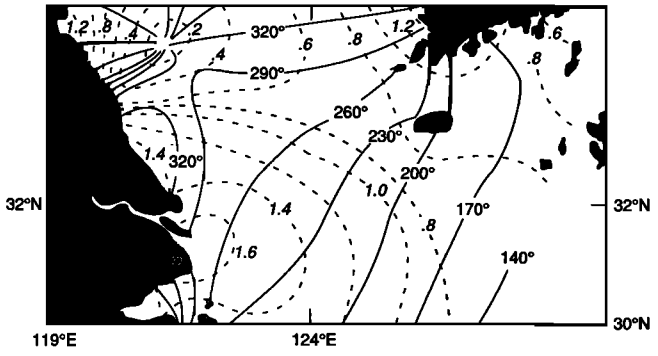

Fig. 5. Computed M_2 elevation cotidal chart from a finite-difference numerical model by *Choi* [1980]. Contours of amplitude (dashed lines, in meters) and phase (solid lines, in degrees with respect to UT) of elevation are given.

To investigate the effect of using basis functions which are closer in form to the normal mode solution of the shallow water equations for the region being studied, we performed several attempts at fitting Kelvin and Poincaré modes that can perfectly represent periodic motions in a semi-infinite rectangular, flat-bottomed channel [*Taylor*, 1920; *Godin*, 1965]. The principal mode of motion in such a channel is composed of the superposition of incident and reflected Kelvin waves, however, the need to satisfy the no-flow condition at the closed end requires the inclusion of an infinite sum of Poincaré waves. The Kelvin mode has zero cross-channel velocity everywhere. Poincaré modes have both along- and cross-channel velocities, and for a given channel configuration, there is a critical frequency below which all modes are evanescent, i.e., they decay away from the closed wall [*Hendershott and Speranza*, 1971]. Here we model the survey region as a channel 830 km wide and 100 m deep (see Figure 7), which results in all Poincaré modes at M_2 frequency being evanescent. This means that away from the reflecting wall, the far-field solution consists only of the Kelvin wave superposition. Although the results given here correspond to modes without dissipation, it is straightforward to include a linear friction parametrization in the shallow water equations for the idealized channel and obtain a similar modal representation [*Rienecker and Teubner*, 1980]. This, in principle, should give extra fitting capabilities to the modes by increasing their flexibility; however, for the present case, the inclusion of reasonable friction values in the problem did not improve the results in any appreciable way.

In practice, the system of equations to solve is of the same form as (7), but in this case, we need to combine the u and v transport parts into one system of equations. The resulting system is complex, although some manipulations can always be made in order to deal only with real numbers. An advantage (perhaps the only one) of using these modes is that both transport components and sea surface elevation have the same analytical form, which simplifies combining current and elevation information in the same analysis. Figure 7 shows the M_2 elevation cotidal chart obtained by projecting the observations onto a model consisting of

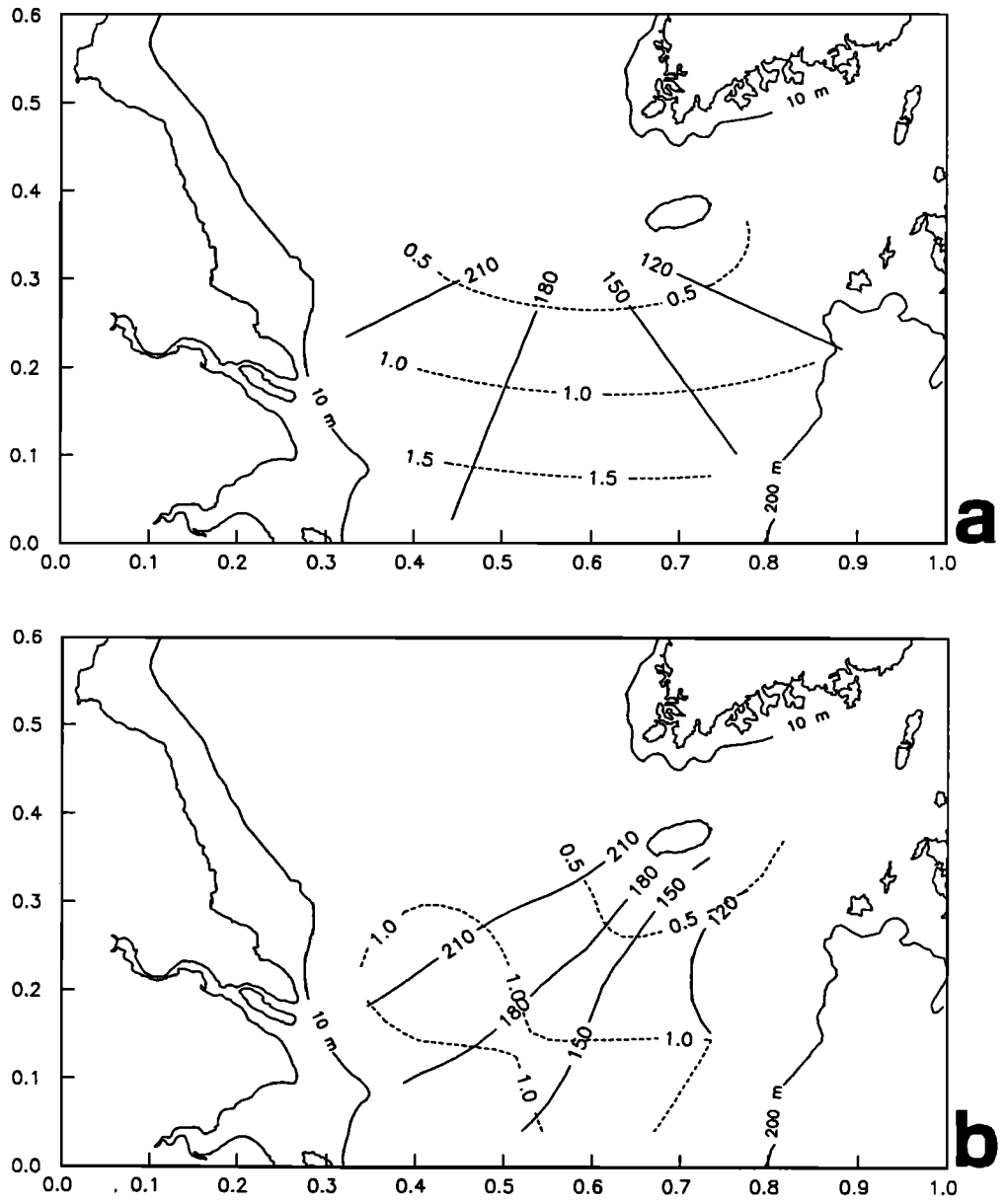

Fig. 6. M_2 cotidal charts obtained from the transport data in Figure 2*a*. Corange lines (lines of equal amplitude) are dashed, in meters. Cotidal lines (lines of equal phase) are solid, in degrees with respect to UT. The analysis is based on (*a*) second-degree polynomials and (*b*) biharmonic basis functions using the five knots shown in Figure 1 by stars. The frequency representative of the semidiurnal band is ~ 30°/hour.

a Kelvin mode (incident plus reflected waves) and the first six Poincaré modes of our idealized channel configuration. While the elevation amplitude and phase patterns have some similarities to those obtained with the other basis functions (Figure 6), there is no dramatic gain by going through the trouble of using these more dynamical basis functions in comparison to arbitrary functions. This lesson was learned long ago in the finite element approach to problems where functions, which are special to the problem by being theoretically perfect, turn out to be practically useless in the approximation application [*Strang*, 1986].

We have described above different attempts to deduce the spatial structure of the tidal motions over the survey region. Although resolving the tidal variability has an importance of its own, one of the main objectives of our analysis effort is to reveal any subtidal flow contained in the ADCP observations. Figure 8*a* shows the steady flow field deduced from the observations (Figure 2*a*) by including a first-degree polynomial approximation in both transport components. Figure 8*b* gives the 95% confidence limits deduced using (11) along with the appropriate Student's t distribution values depending on ν. The combination of these two figures indicates the presence of a steady flow toward the Tsushima Strait south of Cheju Island amounting to about 1 Sv, with essentially no transport in or out of the Yellow Sea proper. Care should be exercised when interpreting the steady part of the model, since any subtidal time variability can be interpreted erroneously as describing a particular steady current pattern. This is one example where there would be a clear advantage in having simultaneous moored observations within the survey region. However, the main feature depicted by the steady transport pattern in Figure 8*a*, i.e.,

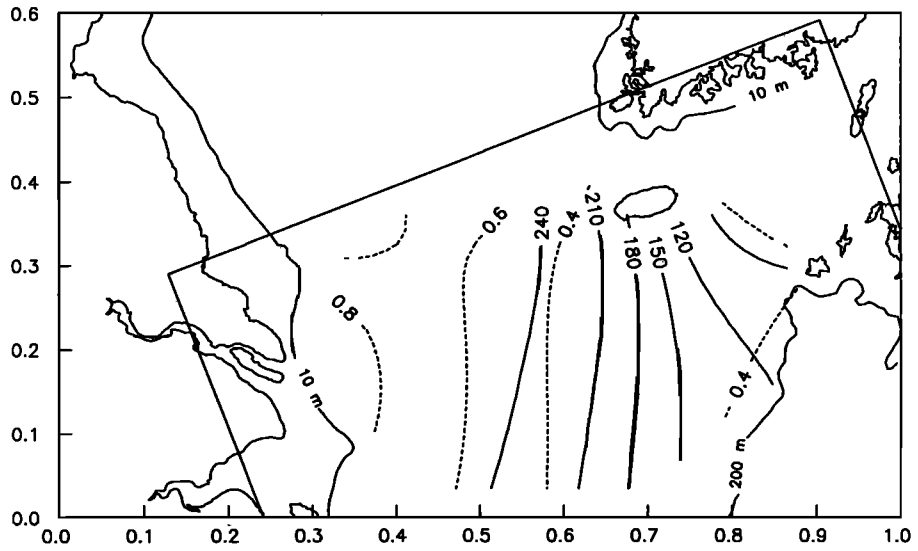

Fig. 7. M_2 cotidal chart approximation using a superposition of Kelvin and Poincaré modes to fit the transport data in Figure 2*a*. Amplitude (dashed lines, in meters) and phase (solid lines, in degrees with respect to UT) obtained using incident and reflected Kelvin waves and the first six Poincaré modes at the M_2 tidal frequency. The outline of the rectangular semi-infinite sea (830 km wide by 100 m deep) used to get the modal structures is shown.

the flow towards the Tsushima Strait appears to be reliably time independent over the length of the survey due to its positioning along the ship's track.

Nitani [1972] and others have argued for the presence of a permanent Yellow Sea warm current originating in the Kuroshio and intruding northward through the East China Sea and along the eastern side of the Yellow Sea. Even though the steady transport pattern in Figure 8*a* does not indicate any such flow, the residual transport field shown in Figure 8*c* suggests a weak coherent jet flowing northwestward south of Cheju Island into the Yellow Sea. The residual field consists of the transport left after the modeled tidal and steady transports are subtracted from the observed ones, i.e., after the flows shown in Figures 2*b* and 8*a* are subtracted from Figure 2*a*, and therefore by construction is orthogonal to both. By choosing smooth functions to approximate the observations, we do not allow for features which are small with respect to the survey area. Moreover, first-order polynomials (such as those used to approximate the steady transports) describe planes that will only resolve features with characteristic dimensions as those of the survey area. Thus the residual transport field can contain useful information and should be examined. In this case, the residual field mainly consists of unresolved tidal motions, some small-scale eddy activity (noise), and evidence of a weak, possibly jetlike flow into the Yellow Sea transporting about 0.06 Sv (over a jet about 20 km wide with transports of about 3 m^2/s). Clearly, additional current data is required to probe the existence and permanence of such small-scale features with any certainty.

3.2. *Amazon Shelf*

Next we will analyze data from several ADCP–CTD surveys conducted over the Amazon shelf during March and May 1990. The Amazon shelf (Figure 9) is quite wide ($\sim$ 250 km) and shallow (average depth $\sim$ 40 m), and is subject to strong forcing by the Amazon River (the world's largest point source of freshwater discharge into the ocean), the semidiurnal tide, and the North Brazil Current (NBC) which flows northwestward over the continental margin with speeds up to 1.5 m/s. The Amazon shelf is presently the focus of A Multidisciplinary Amazon Shelf Sediment Study (AMASSEDS), involving U.S. and Brazilian scientists, designed to investigate physical, geological and chemical processes related to sediment transport through the Amazon dispersal system. As part of AMASSEDS, ADCP data were obtained during (1) two regional scale surveys (each lasting 9 days and sampling along seven cross-shelf transects spanning a 600-km-long section of shelf in front of the Amazon River delta) and (2) several smaller-scale surveys and 24-hour anchor stations made to study frontal processes in the Amazon River plume. Additional current data were obtained from moored current meters deployed at three sites across the shelf during the spring of 1990. Figure 9 shows the main ADCP data station locations for the May 22–31 regional survey and the moored current meter locations. As for the Yellow Sea ADCP data set, we have also chosen here to average every 20 km in space or every hour in time along the ship's track to define main ADCP data stations. See *AMASSEDS Research Group* [1990] for an overview of the AMASSEDS field program and *Geyer et al.* [1991] for a pre-

Fig. 8. (*a*) Steady transport expanded with first-degree polynomials in east and north transport components. The scale is indicated in the lower left-hand corner. (*b*) The 95% confidence limits for the steady transport in Figure 8*a*. (*c*) Residual transport vectors. All three figures have the same scaling factor. Note change of scale in the transports with respect to Figure 2.

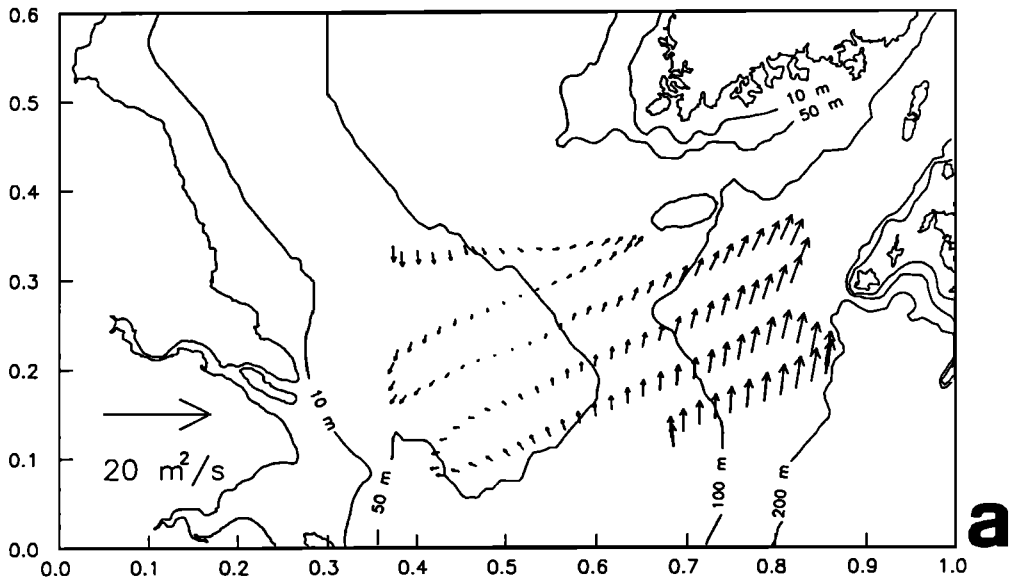
20 m²/s
10 m
50 m
100 m
200 m
a

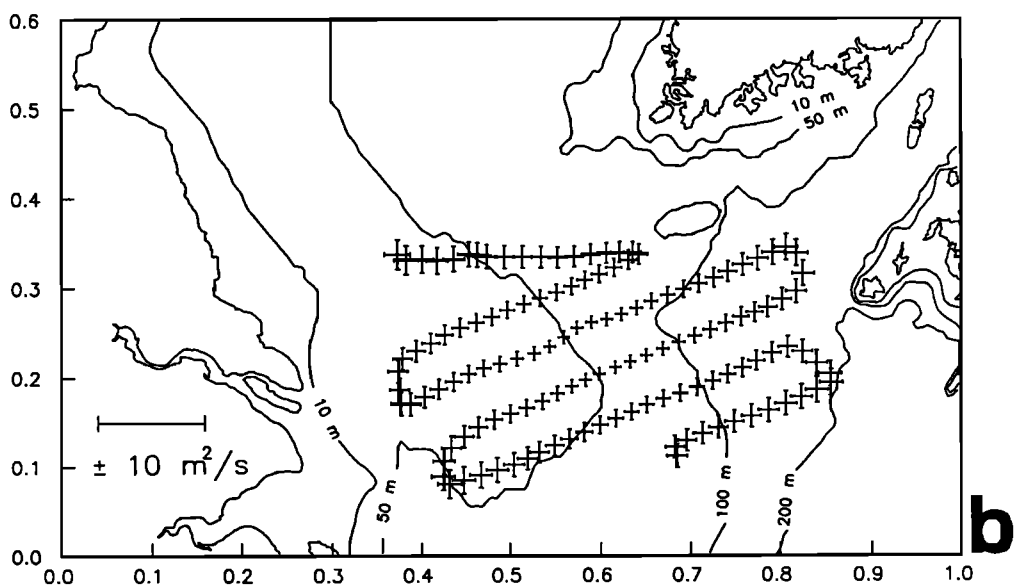
± 10 m²/s
10 m
50 m
100 m
200 m
b

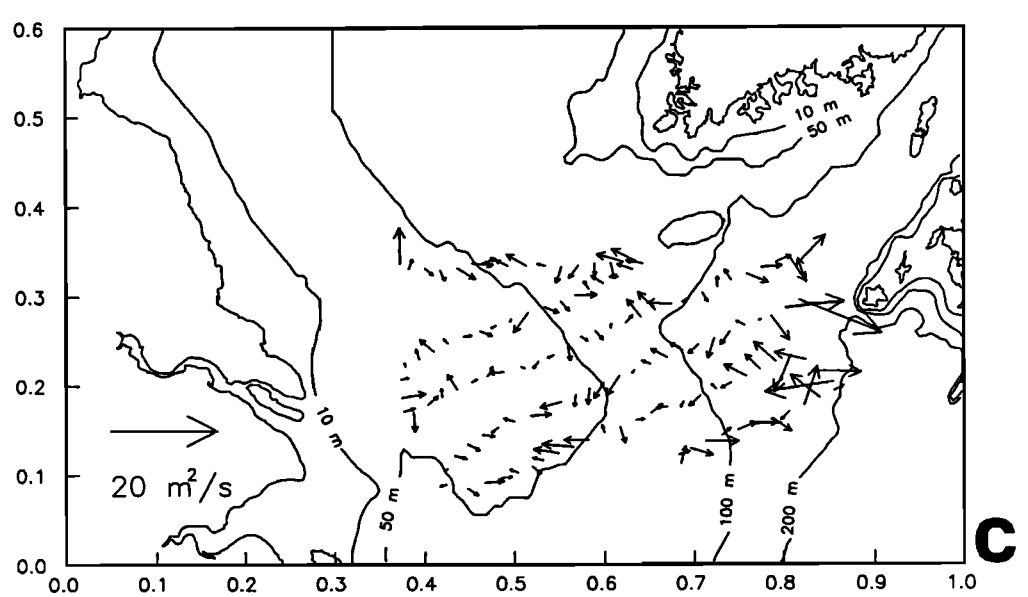
20 m²/s
10 m
50 m
100 m
200 m
c

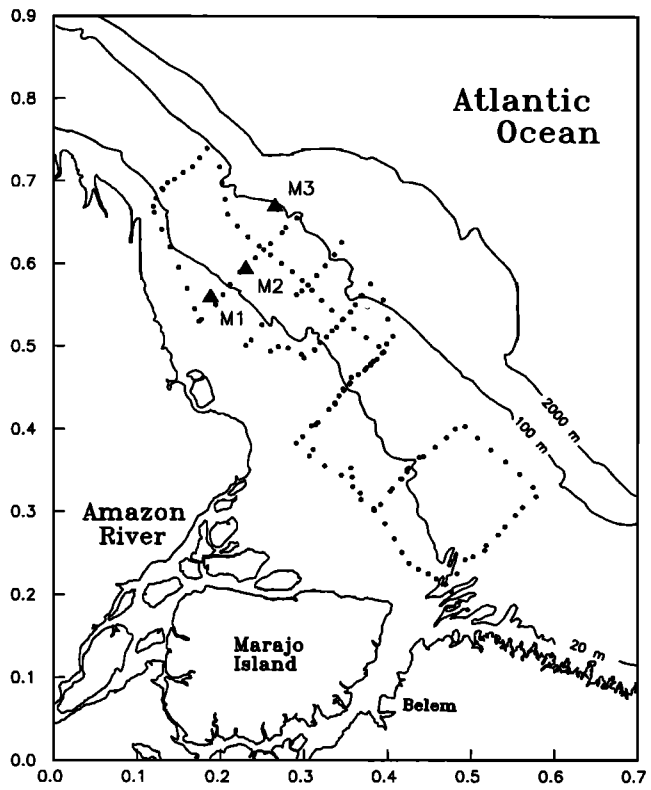

Fig. 9. Map of the Amazon shelf showing the survey track and the location of main ADCP stations during the May 1990 survey. Also indicated are the locations (triangles) of the three mooring sites. The coordinate axes are in 10^6 m, i.e., 100 km for every tick mark, with the origin at 2°S, 52°W. The 20-, 100-, and 2000-m isobaths are shown.

liminary description of the physical oceanographic results from AMASSEDS.

The ADCP data considered here were obtained with a RDI ADCP mounted aboard the R/V *Iselin* using either a 600-kHz or a 150-kHz transducer. Since most of the survey area had depths less than 80 m, the 600-kHz unit was preferred on account of its higher vertical resolution (2-m depth bins as opposed to the 4-m depth bins of the 150-kHz unit). However, over much of the inner shelf, the 600-kHz unit was unable to bottom track, owing (we believe) to near-total absorption of the bottom track ping by the muddy bottom, especially in areas of fluid muds. Once the problem was clearly identified, we switched to the 150-kHz transducer, which was able to bottom track over most of the survey area. Some of the ADCP data without bottom tracking were recovered using GPS navigation. In total, the ADCP data available for analysis from both transducers includes 227 hourly average values between February 28 and March 21, 1990 (from the "March" cruise), and 305 hourly average values between May 22 and June 16, 1990 (from the "May" cruise). Estimated uncertainty in the hourly average ADCP data is about ±2.0% of the true velocity or ±0.5 cm/s, whichever is larger (see appendix). As was mentioned above, additional current data are available from current meters deployed at three mooring sites (see Figure 9): the M1 (inner shelf) site at 17-m depth with two current meters at 3 and 14 m, the M2 (midshelf) site in 60 m of water with three instruments at 3, 30, and 52 m, and the M3 (outer shelf) mooring at 100 m depth with three instruments at 33, 35, and 98 m. Current data from M1 and M2 have a common record length of about 2 months (February 12 to April 13), while the M3 instruments worked for about 4 months (February 10 to June 18).

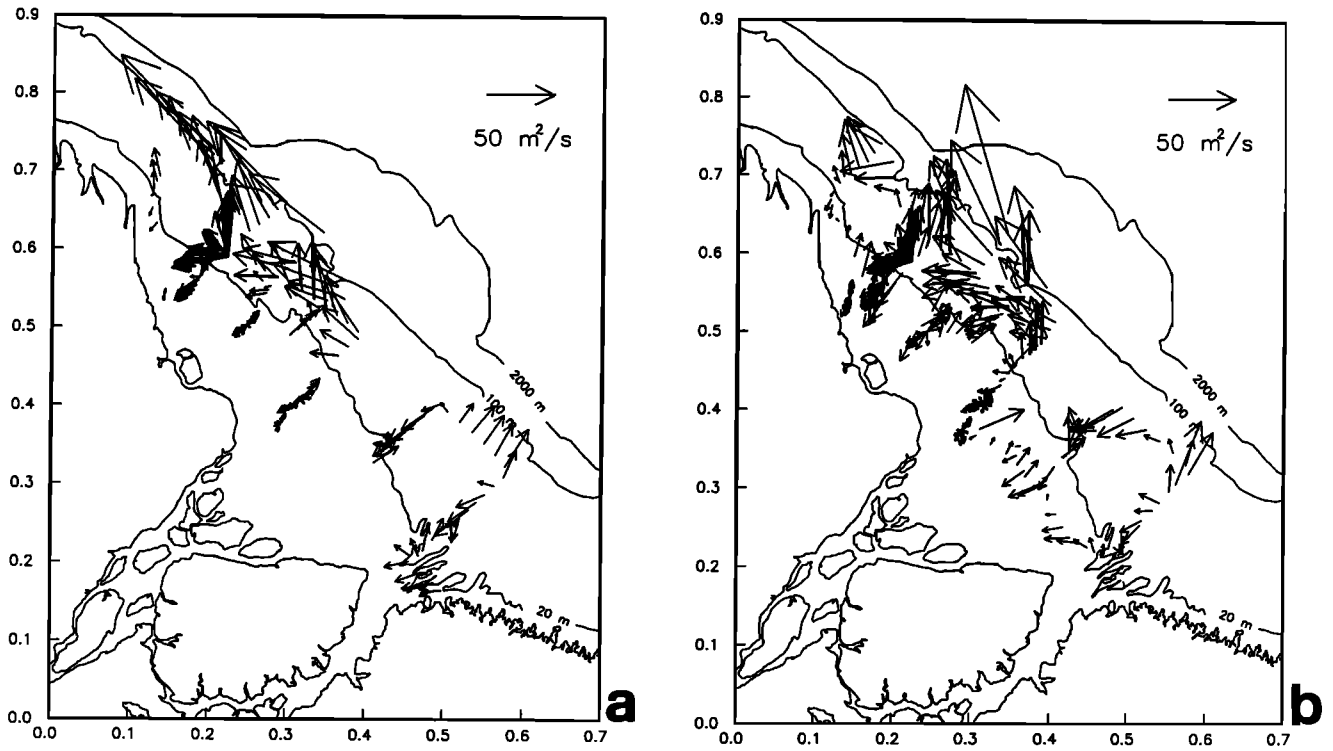

Fig. 10. Vertically integrated transport vectors in square meters per second measured during the (*a*) March and (*b*) May surveys on the Amazon shelf. Data were obtained while the ship was moving and also at anchor stations. The scale is indicated in the upper right-hand corner of each figure.

Although the subtidal flow exhibits vertical shear, both the ADCP and the moored data indicate that the tidal variability is essentially barotropic, so we proceed here with an analysis of the vertically integrated transports. Figure 10 shows the vertically integrated transport vectors obtained during the March and May cruises which include the regional and small scale surveys and anchor stations. The inner and middle shelf transports are strongly polarized in the cross-shelf direction, while toward the outer shelf a strong along-shelf component appears in both surveys. This general description agrees well with earlier observations [*Gibbs*, 1982; *Curtin*, 1986]. Initial trials with both polynomial and biharmonic basis functions for these Amazon data sets indicated that for both the steady and tidal transports the polynomials performed better, i.e., more variance was explained with a lower model order with polynomials than with biharmonics. Therefore we will discuss here only results obtained with polynomials.

First we will deal with the tidal signal. The analysis of the moored observations and existing sea level data shows that the tide over the shelf is principally semidiurnal, with a diurnal to semidiurnal amplitude ratio of ~ 0.1. This permits us to disregard the diurnal band altogether and still account for the main tidal variability by concentrating on the semidiurnal components. Within the semidiurnal band, the S_2/M_2 amplitude ratio is about 0.3, implying an appreciable fortnightly modulation of the shelf tide. It is therefore important to include an S_2 term in the analysis. While the method allows combining all available data irrespective of when and how they were obtained into a single analysis, we will show results for two different data groupings: (1) the combination of all available ADCP data from both cruises, i.e., data shown in Figure 10, which amounts to 532 hourly values, and (2) the combination of all ADCP data plus all moored data from the three sites, amounting to 6502 hourly transport values. This will allow us to compare the ADCP and moored results when analyzed separately or in combination.

When only the ADCP data are considered, the resulting semidiurnal transport vectors, approximated with second-degree polynomials for M_2 and first-degree polynomials for the S_2 terms, are shown in Figure 11. These are an approximation to the transports the ship would have measured if the motions over the shelf were just due to the semidiurnal tide. The modeled semidiurnal tidal transports are basically oriented in the cross-shelf direction, decreasing from about 30 m^2/s near the shelf break (close to the 100-m isobath) to about 10 m^2/s in the inner shelf region (with depths < 10 m). The tidal transport ellipse components for M_2 are given in Figure 12 and for S_2 in Figure 13. Contours of the M_2 semimajor axis indicate the decrease in transport onshore as noticed in Figure 11. Over most of the shelf, the M_2 transport values are around 20 m^2/s. The time of occurrence of the maximum M_2 transports is indicated by the phase contours given in degrees with respect to universal time (UT). These phase lines show that the M_2 signal progresses southward along-shelf north of the Amazon delta, and westward across-shelf in front of the river mouth. The phase contour interval is 30° which amounts to about 1 hour time difference for the principal semidiurnal tide being described. The semiminor axis (Figure 12*b*) indicates that the M_2 transports over the shelf are basically rectilinear, tending to have a slight clockwise rotation toward deep water.

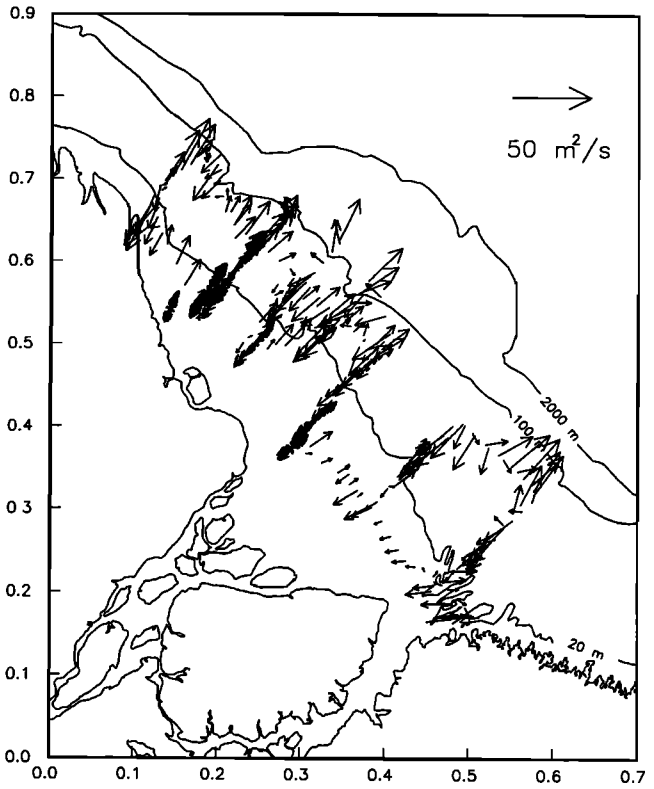

Fig. 11. Semidiurnal tidal transports obtained by simultaneously analyzing all available ADCP data (Figure 10). Second-degree polynomials for M_2 and first-degree ones for S_2 were used to fit the u and v transport components. The values are in square meters per second with the scale given in the upper right-hand corner.

The M_2 transport ellipse orientation confirms the cross-shelf nature of the semidiurnal tidal currents over the shelf. Figure 13 shows the transport ellipse parameters for the S_2 tidal component. Over most of the shelf the S_2 semimajor axis has magnitudes of 6 m^2/s, increasing slightly toward the northeast outer shelf. The phase shows a cross-shelf propagating signal taking a little more than 2 hours to traverse the whole shelf. The semiminor axis (Figure 13*b*) indicates a nearly rectilinear transport over most of the shelf, with some ellipticity and clockwise rotation toward the western outer shelf. The S_2 ellipse orientation, as in the case of M_2, is also basically cross-shelf.

Table 1 lists the tidal ellipse parameters for M_2 and S_2 at the three mooring sites estimated by direct harmonic analysis on the moored data (A), by analysis of all ADCP data (B), and by analysis of all ADCP and moored data together (C). Analyses B and C were done using second-degree polynomials for the steady and M_2 parts and first-degree polynomials for the S_2 term. The close agreement between the results of the moored and ADCP observations analyzed separately is indicative of good consistency between the data sets and also between the methods used. It is interesting to see that the inclusion of the moored data in the analysis, although correcting the tidal phases near the mooring sites somewhat, does not cause a large change in the tidal patterns deduced. This is illustrated by the close similarities of Figure 12 (ADCP) and Figure 14 (ADCP and moored data). The comparison between the S_2 patterns deduced with and without the mooring data, although not shown, is also very

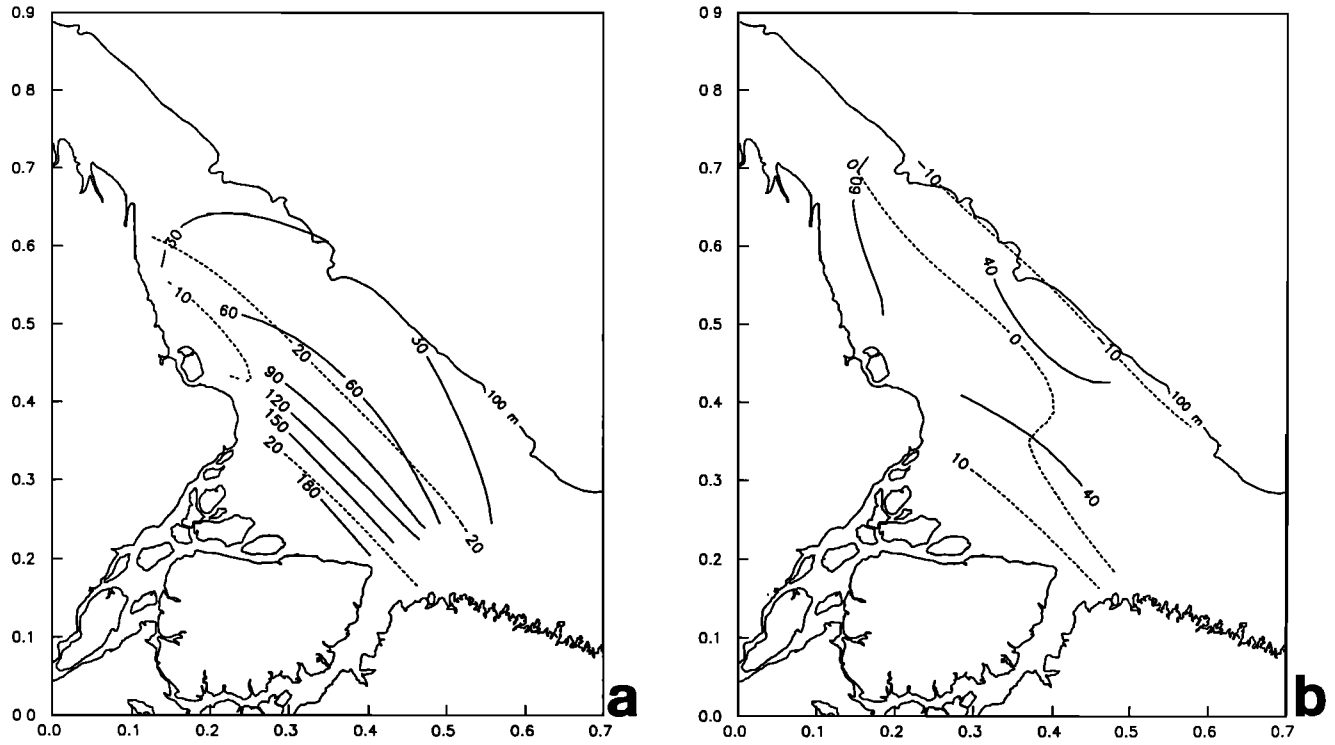

Fig. 12. Contours of the M_2 transport ellipse parameters approximated with second-degree polynomials from only the ADCP data available. (*a*) Semimajor axis (dashed lines) in square meters per second and phase (solid lines) in degrees with respect to UT. (*b*) Semiminor axis (dashed lines) in square meters per second and orientation (solid lines) in trigonometric degrees measured counterclockwise from east.

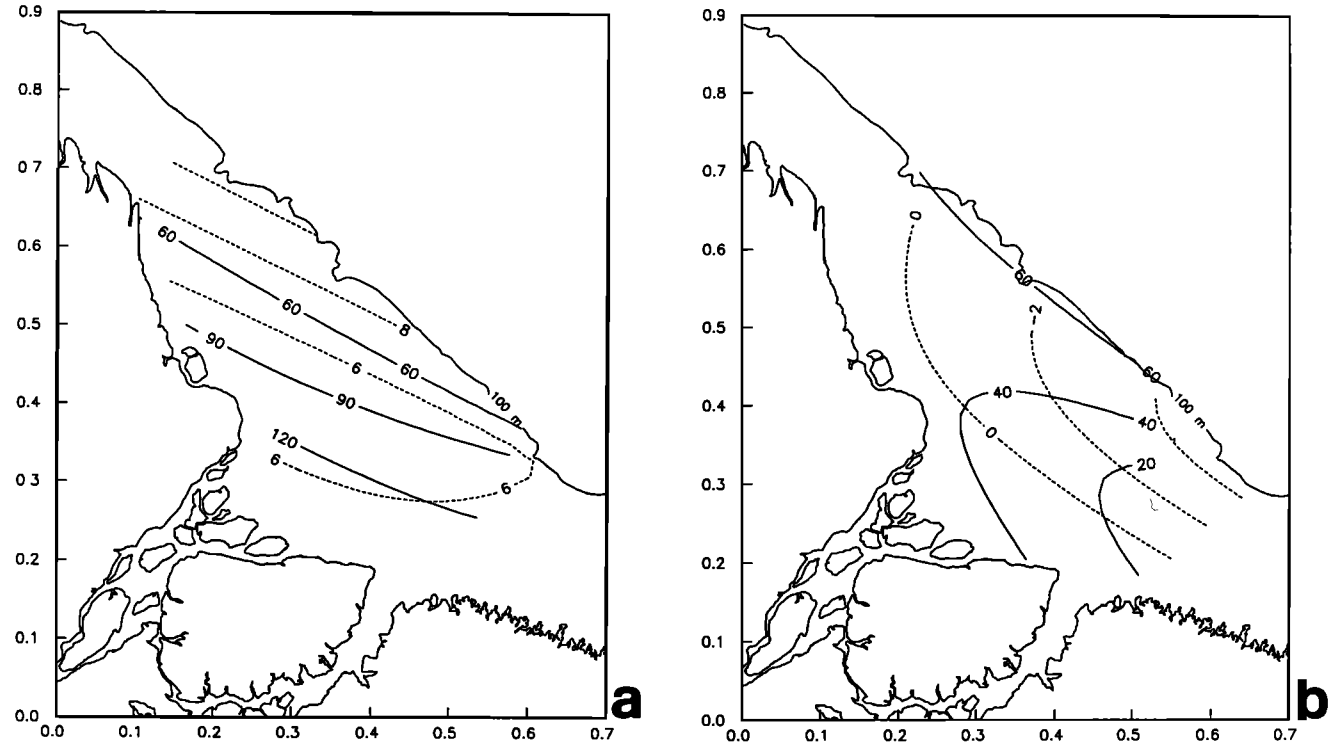

Fig. 13. Contours of the S_2 transport ellipse parameters approximated with first-degree polynomials from only the ADCP data available. (*a*) Semimajor axis (dashed lines) in square meters per second and phase (solid lines) in degrees with respect to UT. (*b*) Semiminor axis (dashed lines) in square meters per second and orientation (solid lines) in trigonometric degrees measured counterclockwise from east.

TABLE 1. M_2 and S_2 Transport Ellipse Parameter Estimates at the Three Mooring Sites From Direct Harmonic Analysis of the Available Moored Data (A), All ADCP Data Using Second-Degree Polynomials for M_2 and First-Degree for S_2 (B), and Combining all ADCP and Moored Data and Using Second-Degree Polynomials for M_2 and First-Degree Polynomials for S_2 (C)

		M_2				S_2			
Analysis	Data Type	M, m²/s	m, m²/s	θ	g	M, m²/s	m, m²/s	θ	g
				Station M1 (1445)					
A	moored	22.8	1.3	58°	30°	7.2	0.1	59°	72°
B	ADCP	17.4	1.7	57°	44°	6.5	0.3	55°	66°
C	ADCP + moored	21.4	1.5	59°	33°	7.7	0.4	58°	72°
				Station M2 (1445)					
A	moored	28.6	2.4	53°	26°	9.6	0.7	51°	61°
B	ADCP	24.8	0.0	51°	39°	7.9	−0.2	57°	53°
C	ADCP + moored	27.7	2.1	52°	28°	7.3	0.0	49°	55°
				Station M3 (3077)					
A	moored	26.1	−4.3	36°	6°	8.2	−1.6	40°	29°
B	ADCP	25.4	−10.0	51°	20°	10.8	−0.4	60°	41°
C	ADCP + moored	25.3	−4.3	36°	7°	8.4	−1.3	41°	32°

M is the semimajor axis; m, the semiminor axis; θ, trigonometric orientation from east; and g is phase in degrees with respect to UT. The number in parentheses after the station name corresponds to the number of hourly values available for analysis at each mooring.

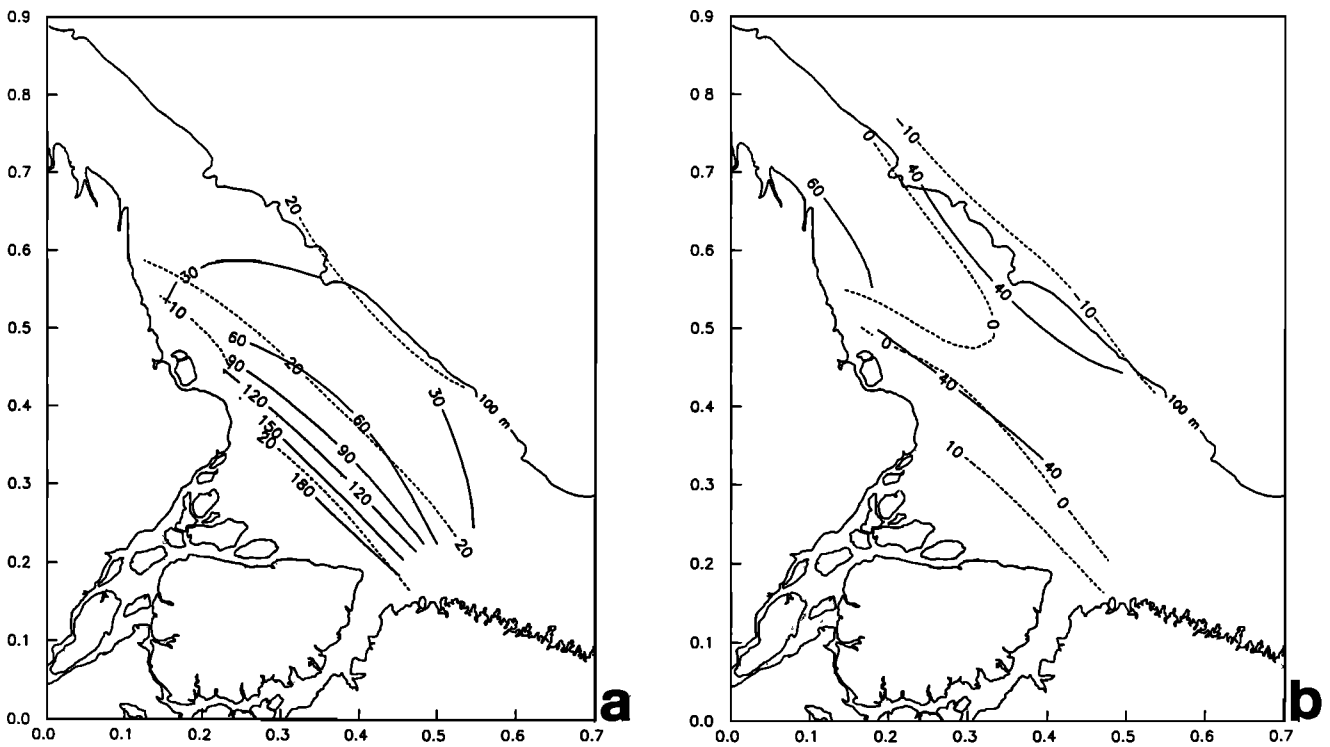

Fig. 14. Contours of the M_2 transport ellipse parameters approximated with second-degree polynomials from the ADCP plus all the moored data available. (*a*) Semimajor axis (dashed lines) in square meters per second and phase (solid lines) in degrees with respect to UT. (*b*) Semiminor axis (dashed lines) in square meters per second and orientation (solid lines) in trigonometric degrees measured counterclockwise from east.

close. Thus for these data sets from the Amazon shelf, the inclusion of moored data has improved the determination of the tidal ellipse parameters around the mooring sites and left the rest of the field essentially unaffected. Apparently once enough data are available to characterize a given tidal constituent at a fixed position, adding more information does not alter the result further provided that the two data sets are consistent.

To conclude our description of the Amazon shelf tide, we show in Figure 15 the M_2 elevation cotidal chart obtained by applying (12) to the ellipse parameters shown in Figure 12. *Schwiderski*'s [1979] analysis of the M_2 tide in this region indicates that at the shelf break, the M_2 phase should be close to 240° and the M_2 amplitude should increase from 0.8 to 1.2 m from northwest to southeast. Figure 15 shows a phase close to 210° and a slight increase southward, between 1 and 1.5 m, along the shelf break. Over the shelf, there is a rapid phase change in the outer shelf with nearly constant elevation, and then an amplitude increase toward the coast with a smoother phase change. It is not clear what the dynamical reasons are for such a behavior, and although Figure 15 has been included here for completeness of presentation, further theoretical work is required to corroborate its veracity.

Perhaps the most interesting phenomenon revealed by the analysis of this ADCP data set is the overwhelming influence of the North Brazil Current over the outer shelf. Although previous work by *Flagg et al.* [1986] and *Richardson and Reverdin* [1987] indicated strong currents in the NBC over the upper slope, very few data on currents over the shelf proper were available prior to AMASSEDS. We used here a second-degree polynomial to model the steady transport components in the March and May ADCP data sets, and show in Figures 16 and 17 the resulting steady transport patterns and the residual vectors for the two data sets. While the residual fields appear to contain some unresolved tidal and eddy motions, the steady transport is dominated by a strong along-shelf current which increases in magnitude from southeast to northwest. Analysis of CTD data collected during each cruise indicates that this along-shelf current carries mostly water of NBC origin. Integration of the steady transport vectors from the shelf break (represented by the 100-m isobath) shoreward gives values of total northwest along-shelf transport over the shelf of about 3.0 and 2.5 Sv for the March and May surveys, respectively. These values are an order of magnitude larger than the maximum river outflow during this time of year. Also, and more importantly, these over-the-shelf flows represent about 25% of the total transport (10 Sv) that the NBC has been predicted to carry during these months [*Philander and Pacanowski*, 1986]. Although there is some difference of the steady transport estimates between the March and May data, both cruises occur at the time when historical ship drift data indicate a minimum strength for the annual variability of the NBC [*Richardson and Walsh*, 1986]. During the late summer and fall months, the NBC is estimated to carry about 30 Sv. What portion of this transport occurs over the shelf during these months remains an important question which we hope to assess with observations from the fourth AMASSEDS cruise in November 1991.

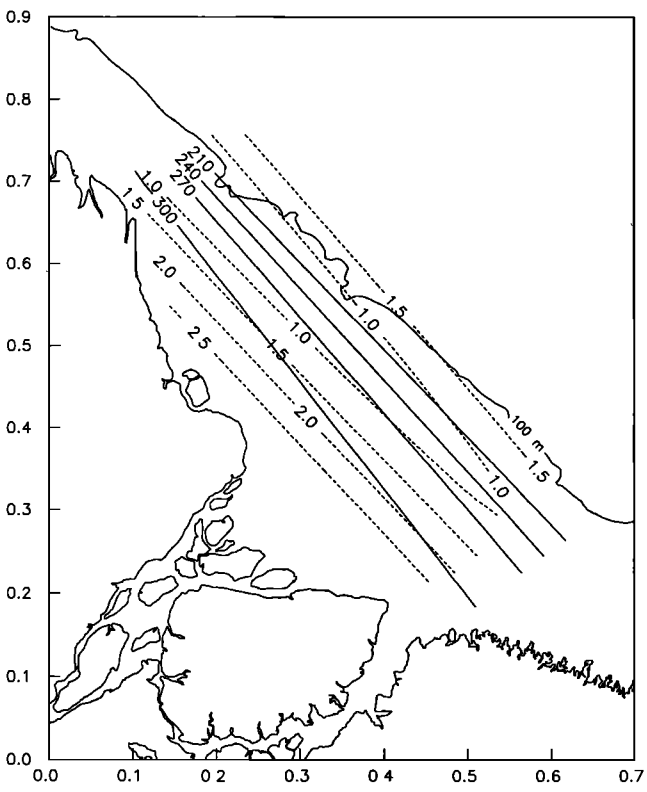

Fig. 15. M_2 elevation cotidal chart obtained from the ellipse parameters of Figure 12 and the continuity relation (12). Shown are contours of amplitude (dashed, in meters) and phase (solid, in degrees with respect to UT).

4. CONCLUSIONS

A simple method is developed to analyze ship-mounted ADCP data acquired during regional hydrographic surveys. The method is based on a spatial interpolation scheme using arbitrary basis functions that can be applied directly to the ADCP data to separate the observed currents into tidal and subtidal components. The method allows additional current data (say, from moored current meters and/or drifters) to be included with the ADCP data in the analysis. The formalism also provides uncertainty estimates of the modeled tidal and subtidal components.

We have applied the method to ADCP data sets from two very different shelf regimes, the mouth of the Yellow Sea where tidal currents are dominant and the Amazon shelf where both subtidal and tidal currents are energetic. The results of the tidal analysis agree well with what is known about the semidiurnal tides in both areas, while the subtidal flow fields deduced from the ADCP data reveal new information about the regional circulation (which will be analyzed and discussed in more detail elsewhere). Experimentation with two simple basis functions (e.g., polynomials and biharmonic functions) and simple analytic representation of idealized regional normal modes indicates that the simplest functions, polynomials, work well and should be used first in any application.

One strength of the proposed method is its ability to include all available data in the analysis. Even though the computation of subtidal flow requires using simultaneous data, the tidal component analysis has no such restriction, and even tidal current predictions at locations within the survey area can be used in the analysis together with the ADCP data. We have conducted some experiments (not

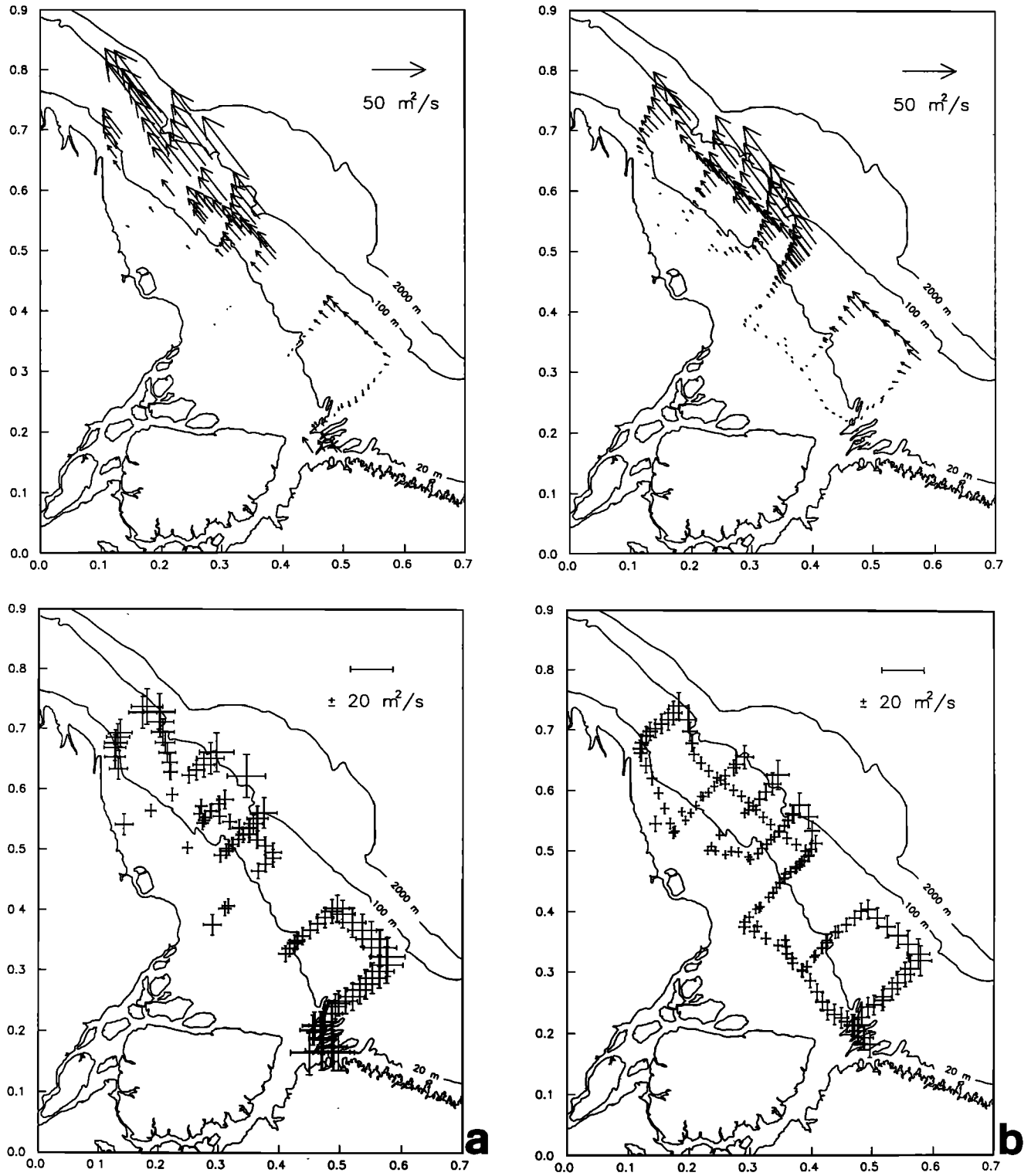

Fig. 16. (Top) Steady part of the observed ADCP transports over the Amazon shelf, with (bottom) the 95% confidence limits for the fitted steady fields, for the (*a*) March and (*b*) May cruises. The units are square meters per second with the scale indicated in each figure, and all panels have the same scaling factor.

discussed in this paper) in which the combination of coastal sea level data with the ADCP data has improved the model description of the tidal pattern. Knowledge of the density field during the survey can also be added if there is evidence that the subtidal flow is in geostrophic balance. The flexibility of the proposed method allows other information to be readily included. C. Chen (unpublished manuscript, 1991) in analyzing ADCP data from short 5-day surveys in the Great South Channel region of the Gulf of Maine has successfully accounted for the effect of unresolved fortnightly modulation by including a time trend in the amplitude of the fitted M_2 term. *Münchow et al.* [1991] have used a model

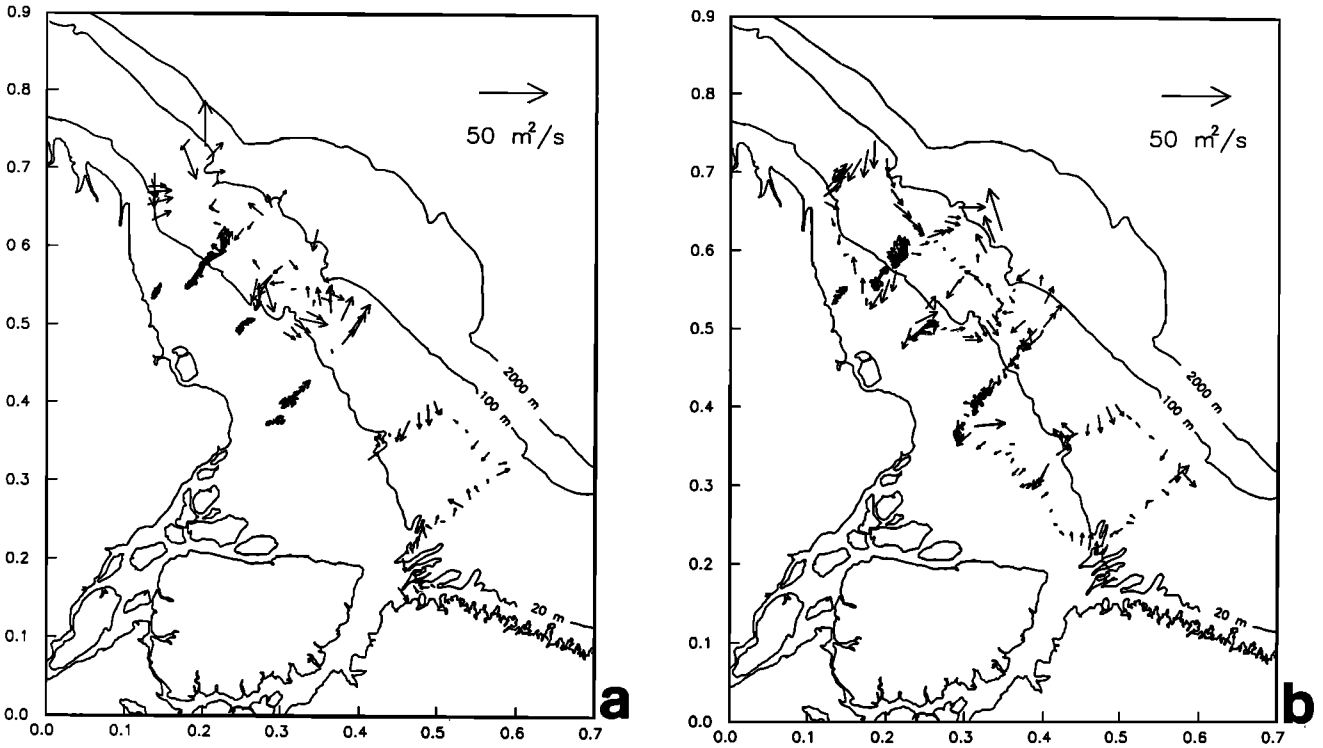

Fig. 17. Residual transport vectors, i.e., unexplained transport variability during the (*a*) March and (*b*) May surveys. The units are square meters per second with the scale indicated in each figure.

of an Ekman layer current profile to fit the vertical structure of the observed tidal currents.

Finally, while this method was originally developed for application to coastal data sets where tidal currents are important, we believe the same or close variants of this approach could be used to separate high-frequency noise (e.g., inertial oscillations) from the subinertial flow of interest. In particular, if time spectra from short sections of the ADCP data reveal a clear spectral gap, then this approach should allow separation of the subinertial signal from the high-frequency noise provided the latter has sufficiently large along-track spatial scales. Recently, *Poulain* [1990] has successfully applied a complex demodulation least squares technique to extract inertial and/or diurnal tidal oscillations from surface drifter observations in the California Current. Although ADCP and drifter data represent different types of measurements, the statistical analysis procedures used for drifters are directly applicable to a set of repetitive ADCP surveys over an area, and by the same token, the method described here is directly applicable to drifter data. These and similar analysis techniques will become more useful as more and more simultaneous ADCP, drifter, and moored array experiments are conducted.

APPENDIX: ESTIMATION OF ADCP UNCERTAINTY

The following procedures were used to estimate the uncertainty in the hourly averaged ADCP current data. Both the East China Sea and the Amazon shelf ADCP data were acquired with bottom tracking, so that following *Joyce* [1989], the true water velocity u_w and ADCP velocity u_d are related by

$$u_w = (1+\beta)\exp^{i\alpha} u_d \quad , \qquad \text{(A1)}$$

where both u_w and u_d are expressed as complex vectors (e.g., $u_w = u_w + iv_w$), and α and β represent the alignment and sensitivity errors, respectively. Estimating the uncertainty in u_w requires estimating the uncertainty in α, β, and u_d; however, this is difficult because gyro and other system errors enter into the uncertainty in u_d as well as in α and β, and comparison with an external absolute velocity reference is required to determine α and β. For the ADCP sampling configurations used in both regions, averaging over approximately 1 hour time intervals reduced the ADCP velocity uncertainty due to acoustic and signal processing considera-

TABLE A1. ADCP Calibration Error Statistics for Both East China Sea and Amazon Shelf Data Sets Based on Comparison of ADCP Bottom Track Velocities With GPS-Derived Velocities

	Mean	s.d.	s.d. Mean
East China Sea (N = 22)			
α	0.463°	0.146°	0.031°
$1+\beta$	0.993	0.017	0.0036
Amazon Shelf (N = 28)			
α	2.797°	3.879°	0.720°
$1+\beta$	0.956	0.087	0.016

For the East China Sea, statistics were computed using 22 samples varying in length from 0.2 to 2.3 hours (average sample length being 1.2 hours). For the Amazon shelf, statistics were computed using 28 samples of 1-hour length. In both cases, α and β were computed using the basic 3-min ADCP bottom track velocities and GPS-derived velocities and equations (10*a*) and (11*a*) from *Joyce* [1989]. Since the mean values of α and β were small in both cases, no corrections using (A1) were applied.

tions (using the manufacturer's specifications of velocity errors) to less than the manufacturer's estimate of long-term accuracy of ±0.5% or ±0.5 cm/s, so we chose to use the latter as the estimated uncertainty in u_d.

To estimate α and β, we compared the ADCP bottom track velocity with the absolute ship's velocity derived from GPS recorded during each survey (Table A1). For the East China Sea survey, statistics for α and β were computed using 22 samples varying in length from 0.2 to 2.3 hours (average sample length was 1.2 hours). For the Amazon shelf surveys, statistics were computed using 28 samples of 1-hour length. In both cases, α and β were computed using the basic 3-min ADCP bottom track velocities and 1-min GPS-derived velocities (with some smoothing for the Amazon shelf data) and equations (10a and 11a) from *Joyce* [1989]. The results (shown in Table A1) indicate that the statistical uncertainty in the mean values of α and β for the East China Sea data set is quite small, resulting in an uncertainty in u_w due to α and β of only ±0.4%. This small uncertainty was due in large part to the high accuracy of GPS (±3–10 m) in the East China Sea during the January 1986 survey. The GPS position accuracy was degraded to about ±100 m during the 1990 Amazon shelf surveys, resulting in an increased (unrealistic) scatter in α and β and a significant increase in the uncertainty in the mean values of α and β. The resulting uncertainty in u_w due to α and β is ±2.1%.

The combined uncertainty in u_w due to all sources was taken as ±0.9% or ±0.5 cm/s for the East China Sea data set and ±2.6% or ±0.5 cm/s for the Amazon shelf data set. Since the correction of the ADCP water velocity u_d in (A1) represents a simple scaling and rotation, this operation may be done either before or after analysis of the ADCP data set. We have chosen to do the analysis discussed in sections 2 and 3 without making any correction using A1 and the mean values of α and β. In cases where poor positioning data causes extreme uncertainty in α and β (as in the Amazon shelf data set), it may be advisable not to correct the ADCP data provided that the mean values of α and β are small, or to use previously determined values of α and β if appropriate. Extreme uncertainties in positioning data should not detract from the inherent accuracy of the ADCP when using bottom tracking.

Acknowledgments. We would like to thank all the people that helped acquire the ADCP data used in this work. In the East China Sea, Tom Lehman, Jack Barth, and Dick Sternberg, even with no previous ADCP experience, obtained an excellent data set which was edited and calibrated by Changchen Chen. Rocky Geyer provided the ADCP anchor station data from the Amazon shelf. Belmiro Castro permitted the use of data from mooring station M3, and Steve Lentz, data from stations M1 and M2 on the Amazon shelf. Andy Solow gave helpful discussion on statistical aspects of the work. The authors also appreciate the detailed reviews which helped clarify the presentation and Barbara Gaffron's editing and typesetting. The first author did part of the work while on a postdoctoral fellowship at the Woods Hole Oceanographic Institution. Data were collected under grants OCE85-01366 and OCE88-12917 from the National Science Foundation, while the analysis work was supported by grants OCE90-17540 and OCE87-16937. Woods Hole Oceanographic Institution contribution 7780.

REFERENCES

AMASSEDS Research Group, A Multidisciplinary Amazon Shelf Sediment Study, *Eos Trans. AGU, 71*, 1771, 1776–1777, 1990.

Candela, J., R. C. Beardsley, and R. Limeburner, Removing tides from ship-mounted ADCP data, with application to the Yellow Sea, in *Proceedings of the IEEE Fourth Working Conference on Current Measurements*, edited by G. F. Appell and T. B. Curtin, pp. 258–266, Institute of Electrical and Electronics Engineers, New York, 1990.

Choi, B. H., A tidal model of the Yellow Sea and eastern China Sea, *KORDI Rep. 80-02*, 72 pp., Korea Ocean Res. Develop. Inst., Seoul, 1980.

Curtin, T. B., Physical observations in the plume region of the Amazon River during peak discharge, III, Currents, *Cont. Shelf Res., 6*, 73–86, 1986.

Davis, J. C., *Statistics and Data Analysis in Geology*, 646 pp., John Wiley, New York, 1986.

Flagg, C. N., R. L. Gordon, and S. McDowell, Hydrographic and current observations on the continental slope and shelf on the western equatorial Atlantic, *J. Phys. Oceanogr., 16*, 1412–1429, 1986.

Foreman, M. G. G., and H. J. Freeland, A comparison of techniques for tide removal from ship-mounted acoustic Doppler measurements along the southwest coast of Vancouver Island, *J. Geophys. Res., 96*, 17,007–17,021, 1991.

Forsythe, G. E., M. A. Malcolm, and C. B. Moler, *Computer Methods for Mathematical Computations*, pp. 192–239, Prentice-Hall, Englewood Cliffs, N. J., 1977.

Geyer, R., and R. Signell, Tidal flow measurements around a headland with a shipboard acoustic Doppler current profiler, *J. Geophys. Res., 95*, 3189–3197, 1990.

Geyer, R., R. Beardsley, J. Candela, B. Castro, R. Legeckis, S. Lentz, R. Limeburner, L. Miranda, and J. Trowbridge, The physical oceanography of the Amazon outflow, *Oceanography, 4*, 8–14, 1991.

Gibbs, R. J., Currents on the shelf of northeastern South America, *Estuarine Coastal Shelf Sci., 14*, 283–299, 1982.

Godin, G., Some remarks on the tidal motion in a narrow rectangular sea of constant depth, *Deep Sea Res., 12*, 461–468, 1965.

Godin, G., *The Analysis of Tides*, p. 53, University of Toronto Press, Toronto, Ont., Canada, 1972.

Hendershott, M. C., and A. Speranza, Co-oscillating tides in long, narrow bays; The Taylor problem revisited, *Deep Sea Res., 18*, 959–980, 1971.

Joyce, T. M., On in situ "calibration" of shipboard ADCPs, *J. Atmos. Oceanic Technol., 6*, 169–172, 1989.

Kosro, P. M., Shipboard acoustic current profiling during the Coastal Ocean Dynamics Experiment, Ph.D. thesis, *SIO Ref. 85-8*, 119 pp., Scripps Inst. of Oceanogr., La Jolla, Calif., 1985.

Lawson, C. L., and R. J. Hanson, *Solving Least Squares Problems*, pp. 36–39, Prentice-Hall, Englewood Cliffs, N. J., 1974.

Lwiza, K. M. M., and D. G. Bowers, Measurements of tidal and residual currents at a front in the North Sea using an acoustic Doppler current profiler (abstract), *Eos Trans. AGU, 71*, 149, 1990.

Münchow, A., R. W. Garvine, and T. F. Pfeiffer, Subtidal currents from a shipboard acoustic Doppler current profiler in tidally dominated waters, *Cont. Shelf Res.*, in press, 1991.

Nitani, T., Beginning of the Kuroshio, in *Kuroshio: Its Physical Aspects*, edited by H. Stommel and K. Yoshida, pp. 129–156, University of Washington Press, Seattle, 1972.

Philander, S. G. H., and R. C. Pacanowski, A model of the seasonal cycle in the tropical Atlantic, *J. Geophys Res., 91*, 14,192–14,206, 1986.

Poulain, P.-M., Near-inertial and diurnal motions in the trajectories of mixed layer drifters, *J. Mar. Res., 48*, 793–823, 1990.

Richardson, P. L., and G. Reverdin, Seasonal cycle of velocity in the Atlantic North Equatorial Undercurrent as measured by surface drifters, current meters, and ship drifts, *J. Geophys. Res., 92*, 3691–3708, 1987.

Richardson, P. L., and D. Walsh, Mapping climatological seasonal variations of surface currents in the tropical Atlantic using ship drifts, *J. Geophys. Res., 91*, 10,537–10,550, 1986.

Rienecker, M. M., and M. D. Teubner, A note on the frictional effects in Taylor's problem, *J Mar. Res., 38*, 183–191, 1980.

Sandwell, D. T., Biharmonic spline interpolation of Geos-3 and Seasat altimeter data, *Geophys. Res. Lett., 14*, 139–142, 1987.

Schwiderski, E. W., Global Ocean Tides, II, The semidiurnal principal lunar tide (M_2), in Atlas of Tidal Charts and Maps, *Tech.*

Rep. TR 79-414, 87 pp., Nav. Surf. Weapons Cent., Dahlgren, Va., 1979.

Simpson, J. H., E. G. Mitchelson-Jacob, and A. E. Hill, Flow structure in a channel from an acoustic Doppler current profiler, *Cont. Shelf Res., 10,* 589–603, 1990.

Strang, G., *Introduction to Applied Mathematics*, p. 428, Wellesley-Cambridge Press, 1986.

Taylor, G. I., Tidal oscillations in gulfs and rectangular basins, *Proc. London Math. Soc., 20*, 148–181, 1920.

R. C. Beardsley, J. Candela, and R. Limeburner, Department of Physical Oceanography, Woods Hole Oceanographic Institution, Woods Hole, MA 02543.

(Received June 18, 1991;
accepted August 23, 1991.)